LBL-10768

Lawrence Berkeley Laboratory
UNIVERSITY OF CALIFORNIA

ENERGY & ENVIRONMENT
DIVISION

A RESIDENTIAL RADON DAUGHTER MONITOR BASED ON ALPHA SPECTROSCOPY

William W. Nazaroff
(M.S. thesis)

May 1980

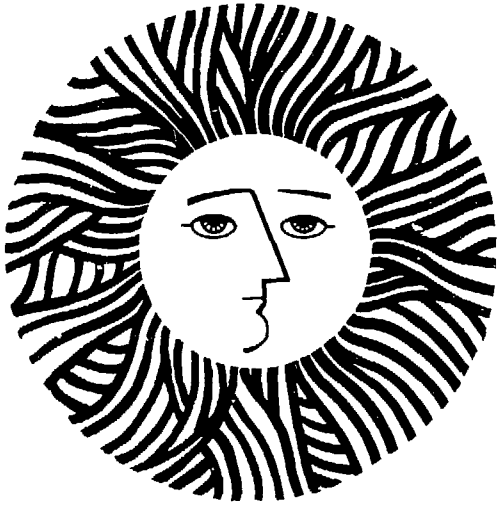

Prepared for the U.S. Department of Energy under Contract W-7405-ENG-48

A RESIDENTIAL RADON DAUGHTER MONITOR

BASED ON ALPHA SPECTROSCOPY

by

William W. Nazaroff

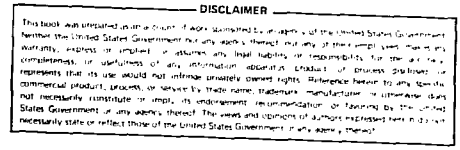

Prepared for the U.S. Department of Energy
under Contract W-7405-ENG-48

ABSTRACT

The radioactive daughters of radon-222 pose a serious indoor air quality problem in some circumstances. A technique for measuring the concentrations of these radioisotopes in air is presented. The method involves drawing air through a filter; then, for two time intervals after sampling, counting the alpha decays from polonium-218 and polonium-214 on the filter. The time intervals are optimized to yield the maximum resolution between the individual daughter concentrations. For a total measurement time of 50 minutes, individual daughter concentrations of 1.0 nanocuries per cubic meter are measured with an uncertainty of 20%. A prototype of a field monitor based on this technique is described, as is a field test in which the prototype was used to measure radon daughter concentrations as a function of ventilation conditions in an energy-efficient house.

*Correction added in proof:

The alpha source originally used for calibrating the RRDM has an uncertainty of twenty percent, rather than five percent as stated on page 37. Recently a five percent uncertain source was used for calibration and the detector efficiency was found to be 14% rather than 12%. Due to this correction, the radon daughter and potential alpha energy concentration measurements presented in Figures 11 and 12 are actually 15% lower than indicated.

ACKNOWLEDGEMENTS

I am grateful for the generous support and assistance throughout this work of many individuals on the staff of the Building Ventilation and Indoor Air Quality (BVIAQ) project at Lawrence Berkeley Laboratory. A. Robb assisted in the design of the power supplies and in the fabrication of the prototype RRDM. Dr. J. Ingersoll was responsible for designing and fabricating the detector vacuum chamber. M. Boegel assisted with the data collection in the field test. K. Revzan did the curve fitting for Fig. 12 and, along with Dr. A. Nero, reviewed the manuscript. J. McCreary, P. Bostelmann and R. Marsh typed the manuscript.

I am especially indebted to Dr. C. Hollowell, the BVIAQ principal investigator, who, because of his technical and administrative excellence, dedication, and perserverance, has been an important inspiration to me.

Finally, I thank my wife, Ingrid, for her unmeasured love and support.

The work described in this manuscript was funded by the Office of Buildings and Community Systems, Assistant Secretary for Conservation and Solar Energy of the U.S. Department of Energy under contract No. W-7405-ENG-48.

CONTENTS

1. [illegible] E. Smith, Molybdenum-Substrate Interactions [illegible] EXAFS Study (Ph.D. Thesis, University of California, 197[illegible]), LBL-[illegible].

*2. W. C. Shih, I. Conformational Analysis of Cyclic Peptides and II. Multinuclear NMR Spectrometer for the Study of Biological Systems (Ph.D. Thesis, University of California, 1979), LBL-10097.

3. [illegible] A. Kirby, A. S. Robertson, M. P. Klein, [illegible] Brown, and P. Eisenberger, Fluorescence Detection of EXAFS: Sensitivity Enhancement for Dilute Species and Thin Films, [illegible], 1977.

*4. [illegible] P. Smith, J. A. Kirby, A. C. Thompson, and M. P. Klein, [illegible], Rev. Sci. Instr. (in press).

*5. Alan S. Robertson, X-ray Absorption Studies of Graphite Intercalates and Metal-Ammonia Solutions (Ph.D. Thesis, University of California, 1979), LBL-9840.

*6. J. V. Acrivos, K. Hathaway, A. S. Robertson, A. C. Thompson, and M. P. Klein, Species Present in Metal-NH_3 Solutions Near the Metal-Insulator Transition, J. Phys. Chem. (in press).

*7. J. V. Acrivos, K. Hathaway, A. J. Bourdillon, A. S. Robertson, and M. P. Klein, Oxidation State of Rubidium [illegible] from X-ray Absorption Spectroscopy, J. Phys. Chem. (in press).

8. [illegible] M. Michaelson, A. F. Horowitz, and M. P. Klein, Head group Modulation of Membrane Fluidity in Sonicated Phospholipid Dispersions, Biochemistry 18, [illegible] (1979).

9. [illegible] Kohler and M. P. Klein, Orientation and Dynamics of Phospholipid Headgroups in Bilayers and Membranes Determined from ^{31}P NMR Chemical Shielding Tensors, Biochemistry 16, [illegible] (1977).

*11. Stanley M. [illegible], Studies of Chromatin [illegible] by Fluorescence Correlation Spectroscopy (Ph.D. Thesis, University of California, 1979), LBL-10119.

*12. [illegible] M. [illegible] and M. P. Klein, Profile of a Focussed Collimated Laser Beam Near the Focal Minimum Characterized by Fluorescence Correlation Spectroscopy, Rev. Sci. Instr. 50, 111-115 (1979).

*13. [illegible] M. [illegible], [illegible] Bartholomew, and M. P. Klein, The Use of Fluorescence Correlation Spectroscopy to Probe Chromatin in the Cell Nucleus, Biochem. Biophys. Acta. (in press).

Abstracts

3. I. CONFORMATIONAL ANALYSIS OF CYCLIC PEPTIDES
   II. MULTINUCLEAR NMR SPECTROMETER FOR THE STUDY OF BIOLOGICAL SYSTEMS

Willy Chao-Wei Shih

Ph.D. Thesis, University of California (1979), LBL-10097

A systematic approach to the employment of ^1H NMR data to the analysis of the solution conformations of small polypeptides is outlined. Two-dimensional homonuclear J-spectra along with the corresponding 45° projections and contour maps simplify the task of homonuclear decoupling experiments, and the assignments of lines is made very straightforward. The vicinal couplings that are likely to vary as the conformation changes are then examined. Spectrum simulations coupled with x-ray data for model systems allow the formulation of Karplus relationships for the vicinal couplings, and solution conformations may then be inferred.

This approach to conformational analysis was applied to an examination of the metal affinities of cyclo-[3-(4-β-aminoethyl)-phenyloxypropanoyl-L-prolyl] and cyclo-[3-(4-β-N-methylaminoethyl)-phenyloxypropanoyl-L-prolyl]. The NMR data revealed that the metal affinity of the former is probably a result of the orientation of both carbonyl groups towards the same face of the ring; the sharply lower affinity of the N-methyl cyclopeptide for divalent cations is likely a result of the carbonyl facing opposite sides of the ring.

Part II of this thesis describes the design approach, major construction details, and the test and characterization procedures associated with the construction of a broadband multinuclear NMR

*See Abstracts.

PAEC	Potential alpha energy concentration (units: working level) numerically given by PAEC = $\underline{X} \cdot \underline{I}$.
$Q_y^{A,D}$	Activity of Ray on filter after (A) or during (D) sampling (nCi).
$\underline{R}$	3-vector $(1, R_1, R_2)$.
R_1	$\frac{I_B}{I_A}$.
R_2	$\frac{I_C}{I_A}$.
s	Decays of ^{218}Po during 2nd count interval divided by ^{218}Po decays during 1st count interval.
$U(t_o)$	Unit step function = 0 for $t > t_o$ = 1 for $0 \leq t \leq t_o$.
V	Volume flow rate of sampling pump (liters per minute).
w	$\frac{M_2}{M_3 - s M_2}$.
$\underline{X}$	3 vector satisfying PAEC = $\underline{X} \cdot \underline{I}$ $\underline{X}$ = (0.00103, 0.00507, 0.00373) .
Δ	$\frac{M_3}{M_2}$.
η	Detector efficiency (counts per disintegration).
θ	Overlap of two alpha channels due to energy absorption by filter and air, defined as counts in ^{218}Po channel due to decays of ^{214}Po divided by counts in ^{214}Po channel due to ^{214}Po decays.
λ_y	Decay constant of Ray (min^{-1}) : λ_A = 0.227, λ_B = 0.0259, λ_C = 0.0352.
σ_y	Standard deviation in measurement of Ray.
σ_{θ,M_i}	Standard deviation of θ or M_i.

1. INTRODUCTION

Air quality is an important environmental concern. Among the consequences of polluted air are adverse health effects, such as increased respiratory disease, ecological disturbances, evidenced by acid rain and increased atmospheric concentrations of carbon dioxide (CO_2), and direct economic loss, from damage to agricultural crops, for example. In the past decade the level of activity on many aspects of air pollution has increased dramatically: identifying and quantifying pollutant sources, studying atmospheric chemistry, monitoring pollutant concentrations, assessing the health impact of pollutant exposures, and regulating pollutant emissions and concentrations. Virtually all this attention has been directed towards outdoor air. Standards have been written to limit emissions from the primary pollutant sources -- industrial processes and combustion for transportation and electricity generation; standards have also been adopted to limit outdoor pollutant concentrations; epidemiologists have attempted to link outdoor pollutant concentrations with adverse health effects.

More recently, it has been shown that substantial sources of air pollutants exist indoors. Of particular concern are radon (^{222}Rn) and its progeny, organic compounds (e.g. formaldehyde), and combustion products (carbon monoxide (CO), oxides of nitrogen (NO_x) and sulfur (SO_x), and fine particulates).[1] Indoor radon sources include soil beneath the building foundation, earth-based building materials, and, in some cases, tap water. Large exposures to radon's radioactive progeny have been linked to an excess incidence of lung cancer in uranium miners. A wide range of organic

compounds arise from certain building materials, furnishings and household cleaning products. For example, formaldehyde, a chemical which causes mucous-membrane irritation and headaches, may be off-gassed by particleboard and urea-formaldehyde foam insulation. Hollowell and Traynor showed that in an experimental kitchen, the concentrations of NO_2 and CO generated by a gas stove could exceed the outdoor air standards.[2] Smoking is another source of combustion products.

Currently not enough is known to determine whether indoor air pollution is a widespread problem. If it is, the implications are quite serious. Regulation, monitoring and control are inherently far more difficult indoors than outside, since even in adjacent structures the pollutant concentrations may be markedly different. Epidemiological studies based on outdoor pollutant measurements are of limited value if the majority of the exposure results from indoor sources. A further and particularly timely consideration is that indoor air quality problems may become worse with the application of energy conservation measures in buildings, especially those which reduce ventilation.

Pollutant measurement techniques are a cornerstone for any assessment of indoor air quality. However, measurement techniques, even for a particular contaminant, vary widely. This paper addresses techniques for measuring concentrations of radon progeny in indoor air.

2. THESIS PURPOSE

The goal of the work reported in this thesis was to develop a portable, relatively inexpensive instrument for field measurements of radon daughters at concentrations typical of indoor air. At the outset there was no commercially available instrument with adequate sensitivity for indoor air measurements of radon daughters.[3] Two field instruments had been developed at research laboratories: the Environmental Working Level Monitor (EWLM) developed at the Massachussetts Institute of Technology and Argonne National Laboratory, and a radon daughter monitor developed in the United Kingdom by Cliff, James and Strong. Both instruments have shortcomings as is discussed in the text.

The starting point for my work was to develop a basis for evaluating and optimizing the sensitivity of radon daughter monitoring techniques. The literature provided a foundation for this development; the evaluation and optimization presented here is more precisely defined and broadly applied than any before.

The analysis revealed that the measurement sensitivity of the Cliff-James-Strong method could be considerably improved upon by counting alpha decays from polonium-218 and polonium-214 separately rather than in sum. Furthermore, this improvement could be realized in an instrument of comparable complexity to the one developed by Cliff, James and Strong. The EWLM, which uses alpha spectroscopy, as well as beta decay measurement, is potentially more sensitive than an instrument based solely on alpha spectroscopy; however, I deemed the gains from beta detection to be insufficient to

offset the additional cost and weight.

A prototype field instrument based on alpha spectroscopy, named the Residential Radon Daughter Monitor (RRDM), was developed. The RRDM was field tested extensively during a two-week experiment in which radon and radon daughter concentrations were monitored under a variety of ventilation conditions in an energy research house. The RRDM proved to be a reliable instrument with sufficient precision for some important information to be gleaned from the results of the field test. With further development, particularly towards reducing size and weight and improving ease of operator use, the RRDM could become a very practical field instrument for low-level radon daughter measurements.

3. BACKGROUND

3.1 Characteristics of Radon and Radon Daughters

Radon (^{222}Rn) is created by the alpha decay of radium (^{226}Ra), a trace element in the earth's crust. Since radon is an inert gas, if the newly formed atom ends its recoil in the interstitial (pore) space of the parent material, it can move to the surface and enter the air. As shown in Figure 1, radon decays by alpha emission to a series of four short-lived radioisotopes (known as radon daughters). These atoms are chemically active and readily attach to aerosols, including particles, in the air. When these aerosols are inhaled, some of them are retained on the surface of the lung. Subsequent decays of the radon daughters to lead (^{210}Pb) result in a radiation dose to adjacent tissue. Of primary concern is the dose due to alpha decays of polonium (^{218}Po and ^{214}Po) since all of the energy of the short-range alphas is deposited near the atomic decay site. Studies of uranium miners demonstrate a correlation between exposure to high concentrations of radon daughters and lung cancer.[4]

A parameter that reflects the health risk associated with exposure to the radon daughters is the potential alpha energy concentration (PAEC), measured in terms of a unit called the "Working Level" (WL). The PAEC is a measure of the alpha decay energy available for exposure of the lungs resulting from the inhalation of radon daughters. This parameter does not depend on the concentration of radon which, being chemically inert, is thought to contribute negligibly to any health risk. One WL is precisely defined

as "any combination of radon daughters in one liter of air such that the ultimate decay to ^{210}Pb will result in 1.3×10^5 MeV of alpha energy."[5] Air containing radon daughters in radioactive equilibrium with 100 nanocuries per cubic meter (nCi/m^3) of radon has a PAEC of 1 WL. Radioactive equilibrium is established if the only removal mechanism for radon daughters is radioactive decay. Under typical indoor conditions, however, radon daughters are removed from the air by ventilation and attachment to surfaces at sufficient rates to result in considerable disequilibrium. When this is the case, more than 100 nCi/m^3 of radon is necessary to generate 1 WL. The relationship between the PAEC and the individual daughter concentrations is given by the expression

$$PAEC = 0.0010\ I_A + 0.0051\ I_B + 0.0037\ I_C \quad , \tag{1}$$

where the PAEC is in units of WL and the daughter activities are in units of nCi/m^3. The coefficients of equation (1), which indicate the relative contribution to risk of the three daughters under equilibrium conditions, are not equal due to two factors. First, since two alpha emissions result from the decay of ^{218}Po to ^{210}Pb, inhalation of an atom of ^{218}Po causes more damage, on average, than inhalation of an atom of ^{214}Pb or ^{214}Bi from which only one alpha is emitted in the decay to ^{210}Pb. The second factor reflects the distinction between number concentration and activity concentration (which I will refer to as activity). The activity of a radioisotope is given by the product of the number concentration and the decay constant, denoted λ. Radioactive equilibrium, which means

equal activity for consecutive elements in a decay chain, thus implies that the number concentrations of the radioisotopes are in inverse proportion to their respective decay constants. For the radon daughters, then, radioactive equilibrium implies that the number concentrations, and therefore the health risk, are greater for ^{214}Pb and ^{214}Bi, which have relatively small decay constants (0.026 and 0.035 $minute^{-1}$, respectively), than for ^{218}Po (λ_A = 0.23 $minute^{-1}$). This factor also explains the absence of the fourth radon daughter, ^{214}Po, from equation (1); its large decay constant (2.5×10^5 $minute^{-1}$) implies an exceptionally small number concentration for reasonable activities. For the definition of the WL, the decay sequence considered ends with ^{210}Pb because its decay constant is so small (0.1 yr^{-1}) that biological processes effect its removal from the lung before it decays.

A useful parameter for expressing the degree of equilibrium between radon and its daughters is the 'equilibrium factor', denoted f. It is defined by

$$f = \frac{100 \text{ PAEC (WL)}}{I_{Rn} \text{ (nCi/m}^3\text{)}} . \qquad (2)$$

The value of f can, in principle, range from zero, if no daughters are present, to one, if the daughter activities are equal to the radon activity. Typical values for buildings lie in the range of 0.3 to 0.7.[6]

The problem of measuring exposure is more complicated than this discussion might suggest. One problem is that retention

characteristics of lung tissue are dependent on the size of the radioactive aerosol. A second but related problem concerns the estimates of dose due to the so-called "unattached fraction" of radon daughters. In atmospheres where the aerosol concentration is low, large fractions of the radon daughters may exist in small molecules or atomic clusters. The unattached fraction is defined for any daughter as the ratio of atoms in this cluster state to the total number of atoms present. These clusters are characterized by high diffusion coefficients compared with aerosols and thus are more effectively collected by the respiratory system. However, there is no consensus as to whether a higher unattached fraction is more harmful, since the clusters may be largely filtered by the nasopharanx passages where they do less harm than in the lung. In spite of these shortcomings, all of the current standards limiting exposure to radon daughters use PAEC as the measure of that exposure.

As instrument requirements are determined in part by the concentrations one wishes to measure, it is instructive to consider the standards for PAEC which have been established. In uranium mines, where natural radon daughter concentrations are typically the highest, the U.S. federal standard limits a miner's integrated exposure to 4 working level months (WLM) per year.[7] One WLM is realized by exposure to one WL for a working month of 173 hours. Assuming an average equilibrium factor of 0.5, this standard corresponds for full-time workers to an average radon concentration in the mine of 67 nCi/m^3. In order to limit exposure of miners outside the mines, the Federal Provincial Task Force on

Radioactivity in Canada established a standard for average PAEC of 0.02 WL in houses in four communities associated with uranium mining and processing.[8] In the United States, the Environmental Protection Agency has recommended a similar standard to the state of Florida for houses built on land reclaimed from phosphate strip mining (resulting in high radium concentration in the soil).[9] Again assuming an equilibrium factor of 0.5, these guidelines correspond to an average radon concentration of 4 nCi/m^3.

3.2 Radon Daughter Measurement Techniques

A number of measurement schemes for radon daughters have been reported in the literature. A broad division exists between those methods that measure only PAEC and those that measure individual daughter concentrations (from which, of course, the PAEC may be computed). Techniques for measuring individual daughter concentrations involve, at the very least, greater computational complexity in data analysis, and may require more hardware to realize than do the PAEC-measuring methods. In many applications, however, one is interested in obtaining more information than simply the total PAEC. Specific examples include measurements in mine atmospheres where the 'age', or degree of radioactive equilibrium, is of interest, and scientific applications where one wishes to study in detail the dynamics of radon daughter behavior. On the other hand, for routine survey work measurement of PAEC is probably adequate.

3.2.1 PAEC Measurements - the Kusnetz Method

The most widely used PAEC technique in both mines and indoor radon daughter studies is based on work by Kusnetz,[10] in which he showed that, between 40 and 90 minutes after sampling, the alpha decay rate of radon daughters per WL on a filter is relatively independent of the degree of radioactive equilibrium. The procedure, then, involves drawing air through a filter for a specified time (up to 10 minutes) at a known flow rate and subsequently measuring the alpha decay rate at some time during the 40 to 90 minute post-sampling interval. In mines, where the radon daughter concentrations are high, the decay rate can be determined by either using an alpha decay ratemeter, or a one minute count with an alpha decay counter. Longer counting intervals can be used to improve the sensitivity for sampling indoor concentrations.[11] Although a number of other PAEC techniques have been proposed, none seems to have the widespread acceptance of methods based on Kusnetz' work.

3.2.2 Individual Daughter Concentration Measurements

The situation with techniques for individual radon daughter measurement at low concentrations is not as clear as for PAEC techniques. Methods originally designed for making individual daughter measurements in mines cannot be easily extended to measure low concentrations as was the Kusnetz PAEC method. Recent advances in integrated circuit technology, on the other hand, have allowed fairly sophisticated instruments to be built with acceptable size and weight for field applications.

All daughter measurement techniques are based on the detection of radioactive decays due to radon daughters that have been

collected on a surface by filtration or electrostatic deposition. In Appendix I, the differential equations for the activity of each daughter on a filter are solved. It is shown that, for a given sampling period (t_o), at any time (t) the activities are linear combinations of the sampled concentrations of that daughter and the previous daughters in the chain. Equations (8A1) state

$$Q_A(t,t_o) = g_{AA}(t,t_o)\ V\ I_A\ ,$$

$$Q_B(t,t_o) = g_{BA}(t,t_o)\ V\ I_A + g_{BB}(t,t_o)\ V\ I_B\ ,$$

$$Q_C(t,t_o) = g_{CA}(t,t_o)\ V\ I_A + g_{CB}(t,t_o)\ V\ I_B$$

$$+ g_{CC}(t,t_o)\ V\ I_C\ ,$$

where the Q's are activities of radon daughters on the filter and the g's are constants which depend only on the sampling period and time.

In the early days of radiation monitoring, measurements of activity were made using decay ratemeters. With advances in electronics, fast and lightweight counters are now available, permitting individual events to be recorded. Most radon daughter measurements are now made with decay counters since the resulting precision is far better than that obtained with a ratemeter. The equations for counts registered due to the decay of a given

daughter during time interval $[t_a, t_b]$ are obtained by integrating equations (8A1);

$$P_A(t_a,t_b,t_o) = \eta_A \, V \, I_A \int_{t_a}^{t_b} g_{AA}(t,t_o) \, dt \, ,$$

$$P_B(t_a,t_b,t_o) = \eta_B \, V \, I_A \int_{t_a}^{t_b} g_{BA}(t,t_o) \, dt + \eta_B \, V \, I_B \int_{t_a}^{t_b} g_{BB}(t,t_o) \, dt \, ,$$

and

$$P_C(t_a,t_b,t_o) = \eta_C \, V \, I_A \int_{t_a}^{t_b} g_{CA}(t,t_o) \, dt + \eta_C V \, I_B \int_{t_a}^{t_b} g_{CB}(t,t_o) \, dt$$

$$+ \eta_C \, V \, I_C \int_{t_a}^{t_b} g_{CC}(t,t_o) \, dt \, , \qquad (3)$$

where $\eta_{A,B,C}$ is the efficiency of detecting decays of ^{218}Po, ^{214}Pb and ^{214}Bi, respectively (counts/disintegration), and $P_{A,B,C}$ is the total count recorded due to the decay of ^{218}Po, ^{214}Pb, and ^{214}Bi respectively, during the time interval (t_a, t_b).

Within the constraint that $I_A \geq I_B \geq I_C$, the airborne concentrations of the daughters are regarded to be independent variables. To determine the concentrations without any prior assumptions about their relative activities, we must measure three independent parameters, i.e. three decay counts, of the filter. In selecting the three counts, three decay types and up to three counting intervals are possible. The only condition to be satisfied is that at least one of the measurements must include decays from ^{214}Bi. We see from equation (3) above, that unless P_C is detected for some time during

the measurement, we obtain no information on ^{214}Bi.

The three decay measurements that can be made are alpha decay from ^{218}Po, alpha decay from ^{214}Po (considered spontaneous emission from ^{214}Bi since the half-life of ^{214}Po is microseconds), and total beta decay from ^{214}Pb and ^{214}Bi. (The beta's cannot be practically distinguished.) It is possible in principle, but unsatisfactory in pratice, to measure the gamma radiation from ^{214}Pb and ^{214}Bi. The difficulties that have precluded the use of gamma detection result from the complex gamma spectra of nuclear decays and from the relatively long range of gamma rays. Because of these properties, good gamma measurement of radon daughters would require pulse-height analysis with high resolution, and would inherently have lower signal levels and higher backgrounds than alpha or beta measurements. In order to appreciate the factors that lead to the choice of which decays to measure, it is necessary to have some understanding of the characteristics of alpha and beta decay. The important differences from a measurement standpoint are in the energy spectrum and the range of the decay particles.

Nuclear decay occurs between states with well-defined energies and, as a result, the decay products share a fixed amount of energy. For alpha decay, only two products result, the alpha particle, which is a doubly ionized helium atom, and the product atom. In order to satisfy conservation of momentum the energy divides between the particles in a fixed manner. Thus, alpha decay from a given radionuclide is monoenergetic. It is this property which allows one to readily do alpha spectroscopy. In beta decay, on the

other hand, three products are created: the beta particle, which is an electron, the product atom, and a neutrino, which is practically undetectable. Since three particles result from the decay, the distribution of energy among the particles is not unique. Beta particles are therefore emitted with any energy between zero and some maximum which is determined by the total energy liberated in the decay. Spectroscopy is thus not a possibility for beta decays with similar energy maxima.

The other important difference is that beta particles have a range which is two orders of magnitude greater than that of alphas (10^{-3}m compared to 10^{-5}m in solids). This has two effects on measurement systems. First, beta detectors must have a larger sensitive volume than alpha detectors, and because the energy loss per distance travelled is considerably less for betas than for alphas, beta measurement faces a larger problem in dealing with backgrounds. The second impact is on filter selection. For alpha spectroscopy, the radioactive particles must be deposited on or near the surface of the filter to avoid substantial energy degradation. For beta measurement this is not an important consideration.

Since the number of counts recorded during any time interval for any decay type is a linear combination of the concentrations of the daughters in the sampled air, we can write general equations for the counts recorded for each of the three measurements.

$$M_1 = (h'_{11}\, I_A + h'_{12}\, I_B + h'_{13}\, I_C)\, V \ ,$$

$$M_2 = (h'_{21}\, I_A + h'_{22}\, I_B + h'_{23}\, I_C)\, V \ ,$$

$$M_3 = (h'_{31} I_A + h'_{32} I_B + h'_{33} I_C) V .$$

In matrix notation this becomes

$$\underline{M} = (H' \cdot \underline{I}) V, \qquad (4)$$

where $\underline{M}$ [$= (M_1, M_2, M_3)$] is the net count vector,

H' is the 3 x 3 conversion matrix between sampled activity and counts, which depends on the type of radiation detected, the counting interval(s) used and the sampling time t_o, the detection efficiency, and

$\underline{I}$ [$= (I_A, I_B, I_C)$] is the vector of concentrations of radon daughters in the sampled air.

If H' is non-singular, eqn. (4) may be inverted to obtain

$$\underline{I} = (K' \cdot \underline{M}) / V , \qquad (5)$$

where $K' = (H')^{-1}$.

For any given measurement scheme, we can use the equations (8A1) and (9A1) along with measured efficiencies to calculated the matrix elements of H'. Inverting H' gives us K' which permits the calculation of the sampled daughter concentrations from the measured counts. Before doing the calculation, the raw counts measured must be corrected for background and, if alpha spectroscopy is used, for overlap of the ^{214}Po and ^{218}Po peaks resulting from energy degradation as the alphas leave

the filter. This will be discussed further in Sections 4.2 and 4.4.

We now examine some of the methods for measuring radon daughter concentrations that have appeared in the literature. The methods selected for examination were chosen because of either common use or the possibility of good sensitivity. We use the following notation for measurement timing.

t_o = the end of the sampling period (i.e. the time at which the pump is shut off),

t_x = the beginning of the first counting interval,

t_1 = the end of the first counting interval,

t_y = the beginning of the second counting interval,

t_2 = the end of the second counting interval,

t_z = the beginning of the third counting interval,

t_3 = the end of the third counting interval.

All times are referenced to the beginning of sampling, and are expressed in minutes.

3.2.2.1. The Thomas-Tsivoglou Method

This method was originally developed in 1953 by Tsivoglou et al.[12] After sampling air for 5 minutes, the total alpha decay rate is measured as a function of time. Decay rates at 5, 15 and 30 minutes after sampling are obtained from a plot

of the count rate versus time. Thomas, in the early 1970's, reported on modifications of this method to allow for counting over finite intervals.[13] Given that the constraint on total measurement time, t_3, is 35 minutes, he suggests the following timing to maximize the sensitivity for ^{218}Po: (t_o, t_x-t_1, t_y-t_2, t_z-t_3) = (5, 7-10, 11-25, 26-35 minutes).

This technique is not sensitive enough for environmental applications; concentrations on the order of tens of nCi/m^3 are required to get reasonable uncertainties. The main difficulty is in obtaining a good number for ^{218}Po. Since the half-life of this isotope is only three minutes, more than one half of the ^{218}Po which is deposited on the filter will have decayed before counting begins with the times Thomas suggested. Furthermore, at reasonable equilibrium conditions, the number concentration of ^{218}Po in the sampled air will be considerably smaller than the number concentrations of the other two isotopes.

3.2.2.2. The Cliff-James-Strong Method (CJSM)

An improvement in the ^{218}Po sensitivity of the Thomas-Tsivoglou method can be made by overlapping the sampling interval and the first counting interval. This idea was first suggested by James and Strong[14] who proposed a two count method measuring total alpha decays for rapidly determining the concentrations of ^{218}Po and ^{214}Bi in mines. Cliff[15] later reported on modifications of this method to allow for three counting intervals and thus for an exact determination of the

three daughter concentrations. Cliff recommends the following timing to obtain maximum sensitivity:

1. $(t_o, t_x\text{-}t_1, t_y\text{-}t_2, t_z\text{-}t_3)$ = (10,0-10,11-26,27-42 minutes),

and

2. $(t_o, t_x\text{-}t_1, t_y\text{-}t_2, t_z\text{-}t_3)$ = (15,0-15,16-36,37-57 minutes).

While the Cliff-James-Strong method offers improved sensitivity over the Thomas-Tsivoglou method, it does pose some difficulties in calibration and requires more complex hardware. In particular, the sampling head must have the alpha detector mounted facing the filter to allow for simultaneous sampling and counting. This geometry makes the air flow pattern much more complex than with a simple open-faced filter holder. It is not clear that particulate collection will be uniform over the filter, or even whether all the particulates will reach the filter.

A difficulty arises in calibration of the Cliff-James-Strong monitor. Calibration of radon daughter monitors is not typically done directly, as it is not at all a trivial matter to generate a constant, known concentration of radon daughters. Instead, detectors are usually calibrated by using a calibrated alpha source, such as americium (^{241}Am) or plutonium (^{239}Pu), uniformly plated on a disk the size of the active area of the filter. One then assumes equal detection efficiency for ^{218}Po and ^{214}Po alphas, that the filters are nearly 100% effective and that the collection is uniform

across the filter. The effectiveness of membrane filters for collecting radon daughters has been demonstrated, however, the difficulty with calibrating the James-Strong monitor is that unless the daughter deposition is uniform across the filter, the actual detection efficiency will be different from that determined with the standard source. The possible magnitude of this effect has not been addressed in the literature.

3.2.2.3. The Environmental Working Level Monitor (EWLM)

The EWLM[16] is an extension of the Instant Working Level Monitor (IWLM) developed at MIT and Argonne National Laboratory by Groer, et al.[17] The IWLM was designed to provide a rapid measurement of radon daughter concentrations in a mine environment. The most recent version is fully automated and can provide measurement results six minutes after the beginning of sampling. The EWLM is basically the same design, with the addition of a more powerful vacuum pump, which draws air at 30-40 liters per minute through the filter. The filter material is formed in a long roll and is automatically advanced after the three minute collection time to a counting station. Here, the alphas are counted by means of a solid-state diffused-junction detector and a single-channel analyzer that discriminates pulses resulting from ^{218}Po and ^{214}Po decays. Beta emissions from ^{214}- and ^{214}Pb are counted using a plastic scintillator coupled to a photomultiplier tube. The alpha detector faces the top of the filter while the beta detector faces the back. The total counting time is three

minutes starting 13 seconds after the end of sampling to allow a stepping motor to advance the filter. Microprocessor control permits preprogramming the sampling repetition rate and total number of samples to be taken.

The high repetition rate of the EWLM has been obtained at the cost of measurement sensitivity, as discussed in Section 4.2. This could, of course, be overcome by using longer measurement times. However, as the EWLM is now implemented, the sampling and counting intervals are fixed. It is not clear how difficult it would be to modify the software to allow variations in the timing.

There is the possibility of some difficulty in using a system with multiple detectors in detailed studies of radon daughter dynamics, due to uncertainties associated with the calibration. In the total alpha counting systems presented above, an error in the calibration would result in a systematic fractional error in the measurement of PAEC and each of the daughters, but this error would cancel if one looked at ratios of daughter activities. In the EWLM, on the other hand, errors in the calibration of either the alpha or beta detector will result in errors in the relative daughter activities as well as in the measurement of PAEC. A further problem is that accurate beta measurements tend to be more difficult to make than accurate alpha measurements. Beta detectors are sensitive to gamma radiation, causing a higher and more variable background (the EWLM accommodates this by

doing a background count during each sampling interval.) Also the efficiency of a beta detector depends on the beta particle end-point energies for the radioisotope of interest; the efficiency differs for ^{214}Pb and ^{214}Bi, again introducing calibration difficulties. Finally, since betas are emitted in a continuous spectrum, the detection efficiency will vary if the threshold voltage for background discrimination drifts.

The size and weight (roughly 30 kg) of the EWLM are handicaps for survey work, although this would not be a problem in a more detailed, longer term study, where the automatic features of the EWLM become very useful.

4. RESIDENTIAL RADON DAUGHTER MONITOR

4.1. Integrated Alpha Spectroscopic Method

The use of alpha spectroscopy alone to measure radon daughter concentrations was first suggested by Martz, et al., in 1969.[18] They recommended a sampling time of 5 minutes, followed by measurements of the alpha decay rate due to ^{218}Po and ^{214}Po at 10 and 35 minutes after the beginning of sampling. Jonassen and Hayes, in 1973, published a study of radon daughter measurement by alpha spectroscopy using finite count intervals, analogous to the Thomas extension of the Tsivoglou method.[19] The recommended time schedule for their method is (t_o, t_x-t_1, t_y-t_2) = (10.0,12.0-15.33,30.0-36.67 minutes).

Alpha spectroscopy improves the detection sensitivity of ^{218}Po to the point where it is no longer the sensitivity constraint. This is because decays of filtered ^{218}Po do not depend on the concentrations of the other daughters, so this atom is measured directly. The hardware required for the alpha spectroscopy is somewhat more sophisticated than for total alpha counting, but not nearly so complex as for the EWLM. Jonassen and Hayes used laboratory equipment: a multichannel analyzer interfaced to a terminal which printed out the spectrum. The diode junction detector was housed in a small vacuum chamber. Vacuum is used to minimize energy degradation as alphas travel from the filter to the detector.

An analysis of sensitivities showed this measurement scheme to be more sensitive than the Cliff-James-Strong method, so this technique was chosen for the Residential Radon Daughter Monitor (RRDM). Considerable computer-aided analysis was undertaken to optimize the timing for maximum sensitivity. A prototype portable instrument was built based on circuits designed for the EWLM and for the RRDM.

A further extension of the integrated alpha spectroscopic method to include counting while sampling was theoretically explored by Tremblay et al.[20] They demonstrate that such a method would offer shorter total measurement times for sensitivity comparable to the Jonassen and Hayes method. However, the details of a sampling head that permits simultaneous alpha spectroscopy and sampling have not been worked out.

4.2 Radon Daughter Monitor Sensitivity Analysis and Optimization

In this section, I develop a basis for calculating the sensitivity of a radon daughter measurement technique. The calculated sensitivity is used for optimizing the counting intervals of the RRDM. These calculations are also applied to the measurement schemes discussd in the previous section, affording comparison of the sensitivity of the various techniques.

First, I introduce the idea of a minimum measurable concentration (MMC). The MMC is defined for any of the daughters

or the PAEC as the concentration in air such that the uncertainty in the measurement is 20% of the concentration. The selection of 20% uncertainty for MMC is a departure from past work. Thomas, who first used this concept to optimize the timing of the Thomas-Tsivoglou method, defined the minimum sensitivity as the concentration at which the uncertainty in the measurement is 50% of the concentration.[21] For optimizing any technique, we shall see that the number selected is irrelevant. However, in terms of the quantitative results there is a difference. Using 50% as Thomas does, one arrives at a minimum detectable as opposed to measurable concentration. Since the RRDM is designed for research rather than for survey applications, it seems more reasonable to use, as a benchmark, a value which can be measured with fair precision. I selected 20% in order to remain in a region where one can ignore contributions to precision due to background, flow rate and timing uncertainties. In residences, radon daughter concentrations can vary over an order of magnitude or more, so that a twenty percent measurement uncertainty is adequate to observe variations resulting from changes in the controlling parameters.

In order to optimize the timing of any technique, we must combine the MMC's for the three daughters into a single parameter. In the past, optimization was done in a rather ad hoc fashion. Cliff optimized his instrument on the basis of ^{218}Po sensitivity.[15] Jonassen and Hayes attempted a manual optimization of the integrated alpha spectroscopic method which

limited both the complexity of their calculations, and the thoroughness of the analysis.[19] The single parameter over which I optimize measurement timing is a weighted average of the individual daughter MMC's, denoted MMCS. It is defined by the following equation:

$$MMCS = (MMCA + MMCB/R_1 + MMCC/R_2)(Q)/3 \ , \tag{6}$$

where

$$R_1 = \frac{I_B}{I_A} \ ,$$

$$R_2 = \frac{I_C}{I_A} \ ,$$

and

$$Q = 0.103 + 0.507\ R_1 + 0.373\ R_2 \ .$$

Equivalently, the MMCS can be expressed as

$$MMCS = \frac{1}{3}\left(\frac{MMCA}{I_A} + \frac{MMCB}{I_B} + \frac{MMCC}{I_C}\right)\ (100\ PAEC).$$

The MMCS is an average over the three radon daughters of one hundred times the PAEC corresponding to the combination of that daughter's MMC and the specified values of R_1 and R_2. This parameter has several useful features. It weights each

daughter by the concentration of ^{218}Po necessary to support it. Empirically, we find that the timing which minimizes MMCS is almost independent of the values of R_1 and R_2. Multiplication by the factor Q reduces dramatically the dependence of MMCS for any particular timing on R_1 and R_2.

In order to calculate the MMC's, I make the approximation that the number of counts observed in any channel for any time interval is an independent, Gaussian distributed variable. Several conditions must be satisfied for counts observed due to radioactive decay to be Gaussian distributed:[22] the probability of an atom producing an observed count must be constant for all atoms of interest, the probability of any atom producing an observed count must be much less than one, and the number of counts detected must be fairly large (20 or more). The first condition is perhaps the biggest stumbling block for radon daughter monitor analysis. This can be seen by considering the probability of observing a count in the ^{214}Po channel when alpha spectroscopy is used. For the radon daughter atoms on the filter this probability will vary widely depending on whether the atom is ^{218}Po, ^{214}Bi, or ^{214}Pb. The second condition of small success probability is not met when, for example, alpha spectroscopy with a high efficiency detector is done for the short-lived ^{218}Po atom. The number of counts observed will be small only when very low concentrations are being sampled so the final condition is not usually constraining. While the errors in uncertainty estimates due to using a simplified analysis are expected to be small, a complete

statistical analysis is beyond the scope of this thesis.

Given this approximation it is possible to calculate the MMC's for any completely determined radon daughter measurement scheme. The details of the calculations for the RRDM, the CJSM, and the EWLM are shown in Appendix II.

Evaluation of the MMC's requires the specification of several variables. First, the product of the sampling flow rate (V) and detector efficiency (η) is specified to be 1.0 (counts per disintegration - liters per minute). The MMC's are inversely proportional to this product, thus the optimization of a given technique is independent of the value assumed. Furthermore, the comparison of different techniques is, to a first approximation, independent of this specification. The practical limit on detector efficiency for any technique is in the range of 0.3 to 0.4 due to geometry and cost considerations. Sampling flow rates are also roughly independent of the measurement technique, with the decision being governed largely by considerations of cost, weight and noise of the pump. The sampling flow rate is further limited for indoor measurements by the requirement that the measurement technique not affect the environment. Sampling flow rates of greater than 60 lpm have been reported for the EWLM with its short sampling time; it is possible that frequent sampling or long sampling times at such high flow rates could disturb the indoor environment sufficiently to affect the results. The second condition to be specified is the degree of equilibrium

of the three daughters. This is denoted by two variables, R_1, and R_2, where

$$R_1 = \frac{^{214}Pb \text{ activity (RaB)}}{^{218}Po \text{ activity (RaA)}}$$

and

$$R_2 = \frac{^{214}Bi \text{ activity (RaC)}}{^{218}Po \text{ activity (RaA)}} .$$

In the analysis presented here, I used three pairs of values for $R_1:R_2$. Conditions of extreme equilibrium are represented by the values $R_1:R_2 = 0.9:0.75$, typical conditions are represented by the values $R_1:R_2 = 0.6:0.4$, and extreme disequilibrium conditions are represented by $R_1:R_2 = 0.3:0.1$.

Another parameter which must be specified in order to evaluate the MMC's for a technique that uses alpha spectroscopy is the energy overlap factor, θ. For the RRDM analysis, a value of 0.05 was used, based on the results of the field test described in Section 4.5. As is discussed in Section 4.4, the value of θ for the RRDM is computed from the data collected with each sample, thus the uncertainty in θ can also be calculated for each sample; the uncertainty in this factor is included in the sensitivity analysis presented in Appendix II. For the EWLM, the overlap is measured when the instrument is calibrated, then assumed constant. Fefe reports values ranging from 0.2 to 0.3 for four recent instruments.[16] The RRDM field test indicated some variation of the overlap from

sample to sample, presumably resulting from varying particulate concentrations and variations in the characteristics of the filters themselves. Based on this information, I assigned for analysis of the EWLM values of 0.2 and 0.02 for the energy overlap and its uncertainty, respectively.

Computer programs were written in Fortran to optimize the RRDM and the CJSM, as well as to compute the MMC's for the EWLM and the Thomas-Tsivogolou method. The RRDM analysis program can be found in Appendix III. The optimization and comparison is done under the constraint of fixed sampling time, t_o, (meaning the time during which the pump is drawing a sample) and fixed total measurement time. It is usually true that one can improve the sensitivity of a technique by going to longer sampling and/or total measurement times. However, there are constraints on both of these numbers. All radon daughter monitors are based on the assumption that the concentations of the daughters do not change during sampling. If a sampling time that is too long is selected, this assumption may not be met. Furthermore, the three minute half-life of ^{218}Po places a practical limit on sampling time. Fifteen minutes is the longest sampling time that has been used. The constraint on total measurement time is a combination of practical application and daughter half-lives. A short total measurement time is desirable from the standpoint of making a quick survey measurement, or in order to obtain a high repetition rate in a detailed study. The daughter half-lives limit total measurement time to about one hour; beyond this only

small gains in sensitivity can be realized.

The results of the optimization and comparison are summarized in Figures 2 through 7 and Table 1.

Figure 2 shows a plot of the MMCS versus total measurement time for the RRDM, under various sampling times. A typical equilibrium condition of $R_1:R_2=0.6:0.4$ is assumed. Below forty minutes, the MMCS is seen to drop rapidly as total measurement time is increased. The gains in sensitivity for sampling times above forty minutes are less pronounced. Thus, a total measurement time between forty and sixty minutes is reasonable. It is further seen that the sensitivity improves for measurement times above forty minutes by using a ten minute sampling time, rather than five minutes. Ten minute sampling also yields better sensitivity than fifteen minutes for total measurement times below sixty minutes.

Figure 3 displays individual components of the MMCS for the RRDM. The sensitivity for ^{214}Pb is the limiting factor for times below 40 minutes, while beyond this point, sensitivity for ^{218}Po becomes the poorest. This figure illustrates the usefulness of the MMCS parameter. It appears to be roughly equal to the arithmetic mean of the MMC's of the three daughters. More importantly, perhaps, is the fact that the individual MMC's track each other well under these conditions; this behavior is consistent with the goal of measuring individual daughter concentrations with roughly equal precision.

Figures 4 and 5 show the effects of varying two of the assumed parameters on the RRDM MMCS. In Figure 4, MMCS is plotted for the RRDM for three different equilibrium conditions. The three conditions chosen span the range of values likely to be encountered. Except for conditions of extreme disequilibrium, the effect of changing the specified equilibrium conditions on the MMCS is small for the RRDM. In Figure 5 it is seen that the influence of small changes in the overlap parameter, θ, is minor, although the optimal timing does depend on θ. For the 0.8 micron millipore filter with sampling flow rates of 10 to 15 liters per minute, θ was measured to be 0.05 ± 0.04. A filter of smaller pore size would likely reduce the overlap, but would require a larger pump to achieve the same flow rates.

Figure 6 is a direct comparison of the RRDM, the CJSM and the EWLM technique[23] assuming a ten minute sampling time and $R_1:R_2=0.6:0.4$. The EWLM technique is seen to give superior results for total times below forty minutes, with a minimum MMCS occuring at roughly 24 minutes. For the EWLM technique, the MMCS rises beyond 24 minutes due to the use of a single measurement time. Since the energy overlap is measured once and assumed constant, rather than measured for each sample, sampling times which are too long cause an increase in the fractional uncertainty of counts recorded in the ^{218}Po channel. Presumably, further improvements in the EWLM technique for long total times could be realized by using a second counting interval and making no a priori assumptions about the

overlap, but this hasn't been investigated. In a direct comparison, the RRDM offers clear advantages over the CJSM. In the range of total measurement times of 40 to 60 minutes, the MMCS of the RRDM is roughly a factor of two below that of the CJSM. Similar results are found at other equilibrium conditions.

Figure 7 is a plot of the optimal intermediate count intervals for the RRDM with a ten-minute sampling time, as a function of the total measurement time. The figure is meant only to show the general shape of the curve, since a different value of θ or a different sampling time would result in different solutions.

Table 1 presents in summary the comparison of the four daughter measurement techniques considered. The Thomas-Tsivoglou method sensitivities were computed using the timing reported by Thomas. Both the EWLM and the CJSM, as designed, provide marked improvements over that method. The integrated alpha spectroscopy method used in the RRDM provides for a further improvement in sensitivity.

As suggested above, this isn't the last word on the subject. For example, the EWLM could be optimized with two counting intervals to improve its sensitivity. Also the use of alpha spectroscopy while sampling has been suggested, although not yet realized in an instrument.

4.3 Prototype Hardware

On the basis of the analysis discussed in the previous section, it was decided to build the RRDM based on integrated alpha spectroscopy. The complexity and expense of the EWLM approach precluded its use, while the CJSM technique did not offer the same level of sensitivity.

A block diagram of the RRDM is presented in Figure 8. A small vacuum chamber contains the solid-state surface barrier detector. The filter to be counted is placed in a holder mounted in a sliding tray. After the tray is pushed into place with the filter directly below the detector, the chamber is evacuated to 4 inches of mercury, absolute, as indicated on the vacuum gauge. Evacuation is easily accomplished in the field in 30 to 45 seconds by means of a small hand-operated vacuum pump.

The detector is biased to +300 VDC. Alpha particles entering the depletion region of the detector generate electron-hole pairs which are separated by the electric field. The electrons appear at the preamp input, where their charge is sensed and converted into a voltage. This voltage is amplified by a unipolar differentiating amplifier. The amplitude of the output pulse is proportional to the energy of the incident alpha particle. The pulses are separated into two streams according to pulse height by a single channel analyzer (SCA). Two five-decade counters record the number of pulses in the two outputs of the SCA. A five-digit display is controlled by a front panel switch to display the counts in either the high- or low-energy channel. Other front panel controls are a

power switch, a reset button, and a count/stop switch. The prototype instrument, pictured in Figure 9, measures 27 cm by 30 cm by 45 cm and weighs 10 kg.

The electronics schematic of the RRDM appears in Figure 10. The charge sensitive preamplifier was designed and built at Lawrence Berkeley Laboratory. It requires both ± 24V and ± 12V power supplies, a disadvantage for use in a field instrument. The output of the preamp is a fast-rising voltage spike with a fairly long tail. Since it is a charge amplifier, pulses can follow each other closely and still pass through the preamp, with a voltage rise that is proportional to charge. The next stage is a differentiating, unipolar amplifier based on two operational amplifiers (op-amps). The op-amp selected (AD503K) has a fairly high slew rate (3 volts/microsecond), and FET inputs for low input bias current. The resistor and capacitor values for this stage were selected by observing the output of the amplifier in the lab. A unipolar pulse with low overshoot was desired, along with a peak output voltage of between three and five volts for the high energy alpha particles.

The next stage is the single-channel analyzer. This circuit was adapted from a design by Keefe, et al., for the EWLM.[16] Pulses are separated according to height by a pair of comparators (LM306). The output of the amplifier is fed to the positive input of the comparators; reference voltages, generated by a potentiometer between the five volt power supply and ground, are at the negative inputs. The reference voltages are adjusted during a calibration

procedure so that one comparator allows only the high energy alpha pulses to pass, while the other allows all alpha pulses to pass. A circuit built from three TTL chips blocks the lower level output when both comparators respond to the pulse.

The two streams of pulses are counted using a pair of 5-decade counters (MC14534B). These chips are designed with the output data time-multiplexed. A one-shot (74LS123) is set up as an astable logic element, and is used to provide the digit-select clock for the counters. The output lines of the counters are tri-state, so the outputs of the two counters are tied together, buffered, and used to drive five display chips. These chips are 5x7 dot-matrix LED displays (HP5082 7300) with BCD input and data latching. The position of a front-panel switch tied to the tri-state control lines determines which channel is displayed.

The power supply circuitry is complicated by the fact that the preamp requires ±24V, mandating the use of a second (stacked) transformer, a second rectifier bridge, and a second pair of large capacitors, as well as the additional voltage regulators. The high voltage used to bias the solid state detector is generated by means of a DC-to-DC converter (VENUS C8T). With five volts input, it generates a center tapped 600 VDC output. This converter easily supplies the input current requirement for the detector which is a few microamps.

4.4 Calibration

The calibration and adjustment of the monitor requires a radium source, a calibrated alpha source with the same geometry as the filter to be used, a pulse-height analyzer and a pulse generator, preferably with two independent channels. First, consider the adjustment of the discriminator settings. The output of the amplifier is connected to the input of the pulse-height analyzer. The radium source is placed in the chamber and counted until a good spectrum exists. Four peaks are evident; in order of decreasing energy, they are ^{214}Po, ^{218}Po, ^{222}Rn, and ^{226}Ra. Next, the pulser is used as input to the preamplifier. While displaying the radium spectrum, counts are accumulated as the pulser amplitude is adjusted until its counts appear in the appropriate energy locations. If a two-channel pulser is used, the two amplitudes should be set so that they fall just above the ^{218}Po peak, and below the ^{226}Ra peak. Thus, the lower amplitude pulse is set at an energy corresponding to pulse from an alpha with an energy of about 3 MeV. The precise value of the lower-level discrimination does not appear important. However, a substantially lower setting would increase the background count rate, while a substantially higher setting would cause some of the ^{218}Po counts to be missed. The upper-level discriminator corresponds to an energy level of about 6.2 MeV. After the pulser has been adjusted, the pulse-height analyzer is disconnected and the display observed with the pulser still used as input. With only the high-amplitude pulses emitted, the high-level comparator reference voltage is adjusted until the pulses are just not counted. The reference voltage is then properly set; its value is recorded for future reference. The process is repeated for the

low-level comparator reference voltage, using the low-amplitude pulses.

The calibrated alpha source is used to determine the efficiency of the detector. Our source had a decay rate known to within five percent, so a measure of counting rate gives an efficiency calibration known to five percent. The detection efficiency of the prototype RRDM is 12%. An efficiency of 25-30% can be achieved with a detector assembly carefully designed to minimize the separation between the detector and the filter.

4.5 RRDM Data Analysis Procedure

In this section, I present the equations necessary to calculate the radon daughter concentrations from data collected with the RRDM. The notation for the four count totals resulting from a measurement are defined in the table below. Note that these values are assumed to be corrected for background.

Alpha Channel

Count Interval	^{218}Po (Low Energy)	^{214}Po (High Energy)
1	D_1	D_3
2	D_2	D_4

The ratio of ^{218}Po decays in the second count interval to those in the first count interval, denoted s, depends only on the times selected,

$$s = \frac{\left[e^{-\lambda_A t_y} - e^{-\lambda_A t_2}\right]}{\left[e^{-\lambda_A t_x} - e^{-\lambda A t_1}\right]} \quad . \tag{7}$$

The energy overlap factor, θ, is then obtained

$$\theta = \frac{(D_2 - s\, D_1)}{(D_4 - s\, D_3)} \quad . \tag{8}$$

Using θ and the count totals, D_1 through D_4, one obtains the corrected count vector, M, as

$$\begin{aligned} M_1 &= D_1 - \theta\, D_3 \ , \\ M_2 &= D_3\ (1 + \theta) \ , \\ M_3 &= D_4\ (1 + \theta) \ . \end{aligned} \tag{9}$$

Since the detection efficiencies for alpha decays from ^{218}Po and ^{214}Po are assumed equal, equation (5) can be written

$$\underline{I} = (K \cdot \underline{M})\ /nV, \tag{10}$$

or equivalently,

$$I_A = \left(\sum_{i=1}^{3} k_{1i} M_i \right) / \eta V$$

$$I_B = \left(\sum_{i=1}^{3} k_{2i} M_i \right) / \eta V$$

$$I_C = \left(\sum_{i=1}^{3} k_{3i} M_i \right) / \eta V \quad .$$

The values of s and the matrix elements k_{ij} for three optimized timing schemes are presented in Table 2. Evaluation of the matrix elements for other timing schemes may be done using the program in Appendix III with some minor modifications. Given the k_{ij}'s, the data analysis can be done in the field with a hand-held calculator.

4.6 Field Test

In September 1979, the RRDM prototype was field tested in a two week experiment in the Energy Efficient Residence (EER) in Carroll County, Maryland. This house was designed to use a minimum amount of energy. Some of its features are a vestibule "air lock" at the front entrance, 2.3 meter (7'-6") ceiling height to reduce interior volume, surface-mounted electrical outlets to avoid penetrating walls, and double-insulating glass plus storm windows. Considerable care was used in caulking and weatherstripping all cracks. As a result the house has a very low infiltration rate, ranging from 0.05 to 0.15 air changes per hour (ach). (One ach means that the amount of air leaking into the structure in one hour equals the

structure volume.) For reference, typical houses in the United States have infiltration rates ranging from 0.5 to 1.5 ach.

In preliminary measurements in the EER, we observed radon concentrations on the order of 20 to 30 nCi/m^3, implying a much higher PAEC than the recommended limit of 0.02 WL for houses built on phosphate reclaimed land in Florida.[9] In addition, there were complaints of excessive humidity in the EER. As a result of these findings, a mechanical ventilation system with heat recovery via an air-to-air heat exchanger was installed in the house. During the first two weeks after the heat exchanger installation, intensive measurements of radon, radon daughters, and air exchange rate were made under a range of ventilation conditions. The RRDM was used extensively to make the radon daughter measurements.

The complete results of this study are reported elsewhere[24]; in this report I summarize the findings obtained with the RRDM and describe the instrument's field performance. During the study approximately 125 measurements were made with the RRDM. A few samples were lost due to mechanical problems with the filter tray. About twenty percent of the samples were counted with incorrect timing due to operator error. (Each sample requires operator intervention at three critical times separated by roughly 10 minutes.) The data from these samples was not lost, however; the data analysis program used to calculate concentrations and uncertainties from the data accepts arbitrary counting times. The mechanical problems arose from two sources. First, if the filter wasn't well-seated before the tray was pushed into the chamber, the

filter would be crushed between the tray and the chamber wall. The second problem arose when the operator broke the chamber vacuum with the tray instead of with the valve; the inrushing air swept the filter out of its seat and plastered it against the detector, necessitating the disassembly of the chamber for cleaning.

Figure 11 presents a summary of the results of the radon daughter measurements. It is a plot of the measurements of PAEC versus time, with the five ventilation conditions labelled. The main feature of the figure is that the PAEC falls below 0.02 WL only when ventilation rates are greater than or equal to 0.6 ach.

The measurements of radon daughter concentrations made on September 15 illustrate the potential usefulness of the RRDM in obtaining a fuller understanding of radon daughter dynamics. The ventilation on this day is due solely to infiltration. The furnace fan, which moves air from the basement through ducts into all of the upstairs rooms, was on throughout most of the two-week experiment, in order to obtain good mixing of the ventilation tracer gas. At 8 AM on September 15, however, it was shut off for a 26-hour period. During this time the radon concentration increased by 30% from 21 nCi/m^3 to 28 nCi/m^3, while the PAEC increased by 200%, from 0.05 WL to 0.15 WL.

The time profile of the three daughters is shown in Figure 12. While the concentration of ^{218}Po increased only slightly over this period, the concentrations of ^{214}Pb and ^{214}Bi increased by a factor of five. Interestingly, the growth of these daughters is well-fitted by exponential growth curves with time constants of 0.07

hr^{-1}, corresponding to the air exchange rate of the house. As the growth of ^{218}Po cannot account for the growth of the two other daughters, and as their decay constants (1.5 and 2.1 hr^{-1}), are much greater than the growth rate it seems that although the equilibrium factor was low throughout the experiment, the furnace fan did not directly remove the daughters. For example, one might speculate that under the given conditions particulates entered or were generated in the house at a fairly constant rate, and that radon daughters attached to particulates did not plate out. As the recirculation system has a coarse filter, it is possible that the particulates were filtered when the fan was operating, thus keeping the radon daughter concentrations low. Under this hypothesis when the furnace fan was shut off, the particulate concentration would have grown with a time constant equal to the air exchange rate, and the ^{214}Pb and ^{214}Bi concentrations would have grown accordingly. The magnitude of this effect would have been smaller for ^{218}Po, since its larger decay constant implies a smaller probability of ^{218}Po atoms interacting with a surface before decaying. This hypothesis is speculative; further work incorporating measurements of particulate levels and more thorough modelling are necessary.

5. CONCLUSIONS

This work extends the state-of-the-art in radon daughter measurements in several directions. The sensitivity calculation and optimization are more thorough and broadly applied than are any in the literature. The measurement of the energy peak overlap for each sample reduces the uncertainty in the results. The prototype instrument described could become the basis for an inexpensive field instrument for radon daughter measurements.

Future development on the RRDM in the near term should include the addition of automatic timing for the counting intervals. This could be accomplished with a simple controller. Timing information could be provided with thumbwheel switches and an internal clock. An additional pair of decay counters would allow complete filter counting without operator intervention.

Another important near-term development goal is the reduction of the size and weight of the instrument. A preamplifier which requires only ± 12V would reduce the weight of the power supply considerably. The vacuum chamber, which is cut from a block of aluminum, is oversized. Another gain could be realized by reducing the size of the case; the current one is about 50% too large.

The sensitivity of the RRDM can be further improved by the careful design of the detector assembly with particular attention to detector - filter spacing.

Less urgent, but still interesting, work could be addressed to the assumptions made in the analysis and calculations: that the

daughter concentrations are constant during sampling, and that the count total observed in any channel during a time interval is a Gaussian-distributed, independent variable.

The most important and perhaps the most difficult work of all is the intelligent application of daughter measurements in addressing the question of indoor radon daughter behavior. More information on radon daughter dynamics could lead to new control techniques and a more precise estimation of the health effects of radon daughter exposure.

REFERENCES AND NOTES

1. C.D. Hollowell, J.V. Berk, C. Lin, W.W. Nazaroff, and G.W. Traynor, Impact of Energy Conservation in Buildings on Health, Lawrence Berkeley Laboratory Report LBL-9379 (June 1979).

2. C.D. Hollowell and G.W. Traynor, Combustion-Generated Indoor Air Pollution, Lawrence Berkeley Laboratory Report LBL-7832 (April 1978).

3. During the course of this work the Harshaw Chemical Co. (Solon, Ohio) announced the availability of the Environmental Working Level Monitor. The commercial instrument weighs 30 kg and sells for $15,000. Python Industries (Ottawa, Canada) has announced a radon daughter monitor based on alpha spectroscopy that also has the capability of measuring thoron daughters. The first units are expected to be available in November 1980 at a cost of $10,000 to $12,000.

4. Federal Radiation Council, "Guidance for the Control of Radiation Hazards in Uranium Mining," Report FRC No. 8 (Revised), Washington, D.C. (1967).

5. R.L. Rock, D.K. Walker, R.W. Dalzell, and E.J. Harris, Controlling Employee Exposures to Alpha Radiation in Underground Uranium Mines, U.S. Bureau of Mines Handbook, Volumes I and II (1970 and 1971).

6. L.R. Haywood, "Selection of a Radon Level Corresponding to 0.02 WL," paper presented at the Third Workshop on Radon and Radon

Daughters Associated with Uranium Mining and Processing, sponsored by the Atomic Energy Control Board of Canada and held at Port Hope, Ontario, March 12-14, 1980.

7. U.S. General Services Administration, Federal Register, 33, 252 (1968).

8. Atomic Energy Control Board of Canada, Information Bulletin 77-2 (April 7, 1979).

9. U.S. General Services Administration, Federal Register, 44, 128 (1979): 38664-38670.

10. H.L. Kusnetz, "Radon Daughters in Mine Atmospheres - A Field Method for Determining Concentrations," Am. Ind. Hyg. Assn. Quart., 85-88 (March 1956).

11. W.W. Nazaroff, An Improved Technique for Measuring Working Levels of Radon Daughters in Residences, Lawrence Berkeley Laboratory Report LBL-9986 (December 1979).

12. E.C. Tsivoglou, H.E. Ayer, and D.A. Holaday, "Occurrence of Nonequilibrium Atmospheric Mixtures of Radon and Its Daughters," Nucleonics, 40-45 (September 1953).

13. J.W. Thomas, "Modification of the Tsivoglou Method for Radon Daughters in Air," Health Physics 19, p. 691 (November 1970).

14. A.C. James and J.C. Strong, "A Radon Daughter Monitor for Use in Mines," Proc. 3rd Int. Cong. IRPA, USAEC CONF 730907, p. 932 (September 1973).

15. K.D. Cliff, "The Measurement of Low Concentrations of Radon-222 Daughters in Air, with Emphasis on RaA Assessment," Phys. Med. Biol. 23, 55-65 (January 1978).

16. D.J. Keefe, W.P. McDowell, and P.G. Groer, The Environmental Working Level Monitor, Argonne National Laboratory Report P7628C (September 1978).

17. P.G. Groer, R.D. Evans, and D.A. Gordon, "An Instant Working Level Meter for Uranium Mines," Health Physics 24, 387-395 (1973).

18. D.E. Martz, D.F. Holleman, D.E. McCurdy, and K.J. Schlager, "Analysis of Atmospheric Concentrations of RaA, RaB and RaC by Alpha Spectroscopy," Health Physics 17, 131-138 (1969).

19. N. Jonassen and E.I. Hayes, "The Measurement of Low Concentrations of the Short-Lived Radon-222 Daughters in the Air by Alpha Spectroscopy," Health Physics 26, 104-110 (1974).

20. R.J. Tremblay, A. LeClerc, C. Mathieu, R. Pepin and M.G. Townsend, "Measurement of Radon Progeny Concentration in Air by α-Particle Spectrometric Counting During and After Air Sampling," Health Physics 36, 401-411 (March 1979).

21. J.W. Thomas, "Measurement of Radon Daughters in Air," Health Physics 23, 783/789 (December 1972).

22. G.F. Knoll, Radiation Detection and Measurement, John Wiley and Sons, New York, 104-144 (1979).

23. Note that the EWLM, as actually implemented, sacrifices some sensitivity for measurement speed, using a 6.2 minute total measurement time. See Table 1.

24. W.W. Nazaroff, M.L. Boegel, C.D. Hollowell, and G.D. Roseme, The Use of Mechanical Ventilation with Heat Recovery for Controlling Radon and Radon-Daughter Concentrations, Lawrence Berkeley Laboratory Report, LBL-10222 (March 1980).

25. R.D. Evans, "Engineers' Guide to the Elementary Behavior of Radon Daughters," Health Physics 17, 229-252 (1969).

APPENDIX I. Derivation of Filter Activity Equations

In this appendix, I derive the equations for the activity of the three radon daughters as a function of time both during and after sampling. The activities for each of the daughters are shown to be linear combinations of the sampled concentrations of the daughter of interest and of the preceeding daughters in the chain. A necessary assumption to obtain this result is that the daughter concentrations are constant during sampling.

The following differential equations describe the buildup of activity of the three daughters on the filter during sampling.

$$\frac{dQ^D_A}{dt} = I_A V - \lambda_A Q^D_A,$$

$$\frac{dQ^D_B}{dt} = I_B V - \lambda_B (Q^D_A - Q^D_B), \qquad (1A1)$$

$$\frac{dQ^D_C}{dt} = I_C V - \lambda_C (Q^D_B - Q^D_C),$$

where

λ_A = decay constant of Po-218 = 0.227 min^{-1},

λ_B = decay constant of Pb-214 = 0.026 min^{-1},

λ_C = decay constant of Bi-214 = 0.035 min^{-1},

V = flow rate of the pump (liters per minute),

$Q^D_{A,B,C,}$ = Activity of the radon daughters on the filter

RADIATION CHEMISTRY AND CHEMICAL EVOLUTION

Richard M. Lemmon

A [illegible] interest of the laboratory has been the [illegible] important compound choline chloride, which, in one crystalline form, is decomposed with extremely high efficiency by ionizing radiation; a second crystalline form shows only average behavior towards ionizing radiation. During the past year we have shown that the [illegible] radiation sensitivity increases rapidly above [illegible], but reaches a maximum around [illegible], well below the temperature, [illegible]°C, of the α-β crystal phase transition.[1] We are also using the techniques of solid-state NMR, employing [illegible], [illegible], and ^{15}N labeled cholines to determine the bond lengths of a number of choline analogs, including those of choline chloride, choline bromide, and choline iodide. This work is supplementing past and present x-ray crystallographic studies designed to uncover the unique facet of choline chloride crystals that result in its remarkable radiolysis behavior.

Research on chemical evolution is increasing our understanding of the chemical events that took place on the prebiotic Earth, about 3.5 to 4.5 billion years ago, events that ultimately led to the appearance of the first living cells. Most scientists regard the appearance of life as an inevitable result of the intrinsic physical and chemical properties of matter. Recent laboratory experiments that simulate presumed prebiotic Earth [illegible] have led to increased understanding of the ways in which biological compounds, such as proteins and [illegible], may have been assembled on our planet's surface. This enhanced knowledge of "prebiotic" [illegible] is also leading to a better understanding of contemporary biological processes.

During 1979, in collaboration with members of the Chemistry Department at Stanford University, we pursued research into the phenomenon of radioracemization, i.e., the racemization of such chiral compounds as the biologically important amino acids, under the effects of gamma rays.[illegible] This research is important for interpretations of the degree of optical rotatory power of amino acids that are found in meteorites. Since the degree of amino acid racemization in fossils is often used to measure the fossils' ages, this work also has implications for geochronology.[4]

In recent years, collaboration with members of the LBL Physics Division has contributed to our understanding of mechanisms which, on the prebiological Earth, may have contributed to a selective advantage of L-amino acids over D-amino acids.[5] That collaboration has continued during 1979 by preliminary experiments designed to show whether highly polarized, accelerated protons exhibit any selectivity in their reactions with L- or D-amino acids.

References

*1. V. Petrouleas, A. Nath, and R. M. Lemmon, Phase Transitions and Radiation Sensitivity of Choline Chloride, Bromide, and Iodide, Rad. Phys. Chem., in press (1980).

*2. W. A. Bonner, N. E. Blair, and R. M. Lemmon, Racemization of Isovaline by γ-Radiation. Cosmological Implications, J. Amer. Chem. Soc. 101, 1049 (1979).

*3. R. M. Lemmon and W. A. Bonner, Radioracemization of Amino Acids, in Origins of Optical Activity in Nature, D. C. Walker, ed. (Elsevier, Amsterdam, 1979), pp. 47-52.

This work was supported by the Division of General Life Sciences, Office of Basic Sciences, U.S. Department of Energy, under Contract No. W-7405-ENG-48.

*See Abstracts.

and

$$Q_C^D(t) = \frac{I_C V}{\lambda_C}(1-e^{-\lambda_C t}) + \frac{I_B V}{\lambda_B}(1-f_{CB}e^{-\lambda_B t}-f_{BC}e^{-\lambda_C t})$$

$$+ \frac{I_A V}{\lambda_A}(1-f_{BA}f_{CA}e^{-\lambda_A t}-f_{AB}f_{CB}e^{-\lambda_B t}-f_{AC}f_{BC}e^{-\lambda_C t}),$$

where

$$f_{yz} = \frac{\lambda_y}{\lambda_y - \lambda_z}.$$

A second set of equations must be solved to determine the activity of the daughters on the filter after sampling. The differential equations and the initial conditions are given below. The superscript A is used to denote that the solutions will be valid only 'after' sampling.

$$\frac{dQ_A^A}{dt} = -\lambda_A Q_A^A, \qquad Q_A^A(t_o) = Q_A^D(t_o).$$

$$\frac{dQ_B^A}{dt} = \lambda_A Q_A^A - \lambda_B Q_B^A, \qquad Q_B^A(t_o) = Q_B^D(t_o). \tag{4A1}$$

$$\frac{dQ_C^A}{dt} = \lambda_B Q_B^A - \lambda_C Q_C^A, \qquad Q_C^A(t_o) = Q_C^D(t_o).$$

Here t_o is the sampling time.

The solution of these equations follows those above. In fact, Evans[25] points out that we can write down the solutions to (4A1) by inspection given (3A1) and the observation that

$$Q_A^A(t) = Q_A^D(t) - Q_A^D(t-t_o),$$

$$Q_B^A(t) = Q_B^D(t) - Q_B^D(t-t_o), \qquad (5A1)$$

and $$Q_C^A(t) = Q_C^D(t) - Q_C^D(t-t_o).$$

Equations (5A1) can be understood by performing the following thought experiment. Imagine that for time t=0 to time $t=t_o$ one samples by pulling air through filter #1. At t_o filter #2 is placed in the sampling train immediately before filter #1. Assume that both filters are 100% effective. The total activity of isotope X on the two filters is then given by $Q_X^D(t)$, while the activity of X on filter #2 is given by $Q_X^D(t-t_o)$. Therefore, the activity of X on filter #1 is given by $Q_X^D(t)-Q_X^D(t-t_o)$, which is identical to equations (5A1).

Writing out the solutions to (4A1) explicitly, we find

$$Q_A^A(t) = \frac{I_A V}{\lambda_A}(e^{-\lambda_A t})(e^{\lambda_A t_o} - 1), \qquad (6A1)$$

$$Q_B^A(t) = \frac{I_B V}{\lambda_B}(e^{-\lambda_B t})(e^{\lambda_B t_o} - 1) + \frac{I_A V}{\lambda_A}(f_{BA}(e^{-\lambda_A t})(e^{\lambda_A t_o} - 1) + f_{AB}(e^{-\lambda_B t})(e^{\lambda_B t_o} - 1)),$$

$$Q_C^A(t) = \frac{I_C V}{\lambda_C}(e^{-\lambda_C t})(e^{\lambda_C t_o} - 1)$$
$$+ \frac{I_B V}{\lambda_B}(f_{CB}(e^{-\lambda_B t})(e^{\lambda_B t_o}-1)+f_{BC}(e^{-\lambda_C t})(e^{\lambda_C t_o}-1))$$
$$+ \frac{I_A V}{\lambda_A}(f_{BA}f_{CA}(e^{-\lambda_A t})(e^{\lambda_A t_o}-1)$$
$$+f_{AB}f_{CB}(e^{-\lambda_B t})(e^{\lambda_B t_o}-1)+f_{AC}f_{BC}(e^{-\lambda_C t})(e^{\lambda_C t_o}-1)).$$

Equations (3A1) and (6A1) can be expressed as a single set of activity equations.

$$Q_A(t,t_o) = U(t_o)\, Q_A^D(t) + (1-U(t_o))\, Q_A^A(t),$$

$$Q_B(t,t_o) = U(t_o)\, Q_B^D(t) + (1-U(t_o))\, Q_B^A(t), \qquad (7A1)$$

$$Q_C(t,t_o) = U(t_o)\, Q_C^D(t) + (1-U(t_o))\, Q_C^A(t),$$

where $U(t_o)$ is the unit step function defined as

$U(t_o) = 0$ for $t > t_o$,

and

$U(t_o) = 1$ for $0 \leq t \leq t_o$.

Finally we observe that equations (7A1) are linear in I_A, I_B and I_C. We can rewrite (7A1) in the following form.

$$Q_A(t,t_o) = g_{AA}(t,t_o) \; V \; I_A.$$

$$Q_B(t,t_o) = g_{BA}(t,t_o) \; V \; I_A + g_{BB}(t,t_o) \; V \; I_B. \tag{8A1}$$

$$Q_C(t,t_o) = g_{CA}(t,t_o) \; V \; I_A + g_{CB}(t,t_o) \; V \; I_B + g_{CC}(t,t_o) \; V \; I_C.$$

The functions g_{yz} depend only on the constants $\lambda_A, \lambda_B, \lambda_C$, the sampling time t_o, and the time t. Thus for a given t_o, the activity of each of the daughters on the filter is at any time, t, a linear combination of the particular daughter and the previous isotopes in the decay chain. Writing out the functions g_{yz} explicitly, we have

$$g_{AA}(t,t_o) = \frac{1}{\lambda_A} \left((e^{-\lambda_A t})(e^{\lambda_A t_o} - 1) + U(t_o)(1 - e^{-\lambda_A (t-t_o)}) \right)$$

$$g_{BB}(t,t_o) = \frac{1}{\lambda_B} \left((e^{-\lambda_B t})(e^{\lambda_B t_o} - 1) + U(t_o)(1 - e^{-\lambda_B (t-t_o)}) \right)$$

$$g_{CC}(t,t_o) = \frac{1}{\lambda_C} \left((e^{-\lambda_C t})(e^{\lambda_C t_o} - 1) + U(t_o)(1 - e^{-\lambda_C (t-t_o)}) \right)$$

$$g_{BA}(t,t_o) = \frac{1}{\lambda_A} \left(f_{BA}(e^{-\lambda_A t})(e^{\lambda_A t_o} - 1) + f_{AB}(e^{-\lambda_B t})(e^{\lambda_B t_o} - 1) \right)$$

$$+ U(t_o)(1 - f_{BA}(e^{-\lambda_A (t-t_o)}) - f_{AB}(e^{-\lambda_B (t-t_o)})) \tag{9A1}$$

$$g_{CB}(t,t_o) = \frac{1}{\lambda_B}\left(f_{CB}(e^{-\lambda_B t})(e^{\lambda_B t_o}-1)+f_{BC}(e^{-\lambda_C t})(e^{\lambda_C t_o}-1)\right.$$

$$\left.+U(t_o)(1-f_{CB}(e^{-\lambda_B(t-t_o)})-f_{BC}(e^{-\lambda_C(t-t_o)})\right)$$

$$g_{CA}(t,t_o) = \frac{1}{\lambda_A} f_{BA}f_{CA}(e^{-\lambda_A t})(e^{\lambda_A t_o}-1)+f_{AB}f_{CB}(e^{-\lambda_B t})(e^{\lambda_B t_o}-1)$$

$$+f_{AC}f_{BC}(e^{-\lambda_C t})(e^{\lambda_C t_o}-1)+U(t_o)(1-f_{BA}f_{CA}(e^{-\lambda_A(t-t_o)})$$

$$-f_{AB}f_{CB}(e^{-\lambda_B(t-t_o)})-f_{AC}f_{BC}(e^{-\lambda_C(t-t_o)})$$

All of the functions g_{yz} are of the form $a_{yz}(t,t_o)+U(t_o)b_{yz}(t-t_o)$.

Appendix II Calculation of Minimum Measurable Concentrations For Radon Daughter Monitors

The basis of all of the calculations of minimum measurable concentration is the approximation that the number of counts in a particular channel for a specified time interval has a Gaussian distribution and is independent of the number in another channel or time interval. If we have a function of some Gaussian distributed independent variables, a_i,

$$b = f(a_1, \ldots, a_n),$$

then the variance in b is given by

$$\sigma_b^2 = \sum_{i=1}^{n} \left[\frac{\partial f}{\partial a_i}\right]^2 \sigma_{a_i}^2 \quad . \tag{1A2}$$

For counting experiments, the variance in the number of counts observed simply equals the number of counts.

$$\sigma_{D_i}^2 = D_i$$

With this as a basis, we can proceed to calculate the minimum measurable concentrations for the daughter measurement techniques.

Residential Radon Daughter Monitor (RRDM)

The RRDM has two counting intervals, and two alpha counters. The elements of the raw-count vector are defined by the following table:

Alpha Channel

Count Interval	^{218}Po (Low energy)	^{214}Po (High energy)
1	D_1	D_3
2	D_2	D_4

The variable s, represents the ratio of ^{218}Po decays in the second count interval to those in the first count interval.

$$s = \frac{\left[e^{-\lambda_A t_y} - e^{-\lambda_A t_2}\right]}{\left[e^{-\lambda_A t_x} - e^{-\lambda_A t_1}\right]} \quad . \tag{2A2}$$

The energy overlap factor, θ, is then obtained as

$$\theta = \frac{(D_2 - s\, D_1)}{(D_4 - s\, D_3)} \quad . \tag{3A2}$$

For the calculation of MMC's, θ is an input parameter.

The corrected count vector M becomes [eqn. (4A2)]

$M_1 = D_1 - \theta D_3$ = Counts due to ^{218}Po decays in first time interval,

$M_2 = D_3\,(1 + \theta)$ = Counts due to ^{214}Po decays in first time interval, and

$M_3 = D_4\,(1 + \theta)$ = Counts due to ^{214}Po decays in second time interval.

These equations are inverted to find

$$D_1 = M_1 + M_2 \frac{\theta}{1 + \theta}$$

$$D_2 = s\, M_1 + M_3 \frac{\theta}{1 + \theta}$$

$$D_3 = \frac{M_2}{1 + \theta} \tag{5A2}$$

$$D_4 = \frac{M_3}{1 + \theta} .$$

For specified equilibrium conditions R_1 and R_2 we define [eqn. (6A2)]

$$w = \frac{M_2}{M_3 - s\,M_2} = \frac{h_{21} + R_1h_{22} + R_2h_{23}}{\left(h_{31} + R_1h_{32} + R_2h_{33}\right) - s\left(h_{21} + R_1h_{22} + R_2h_{23}\right)}$$

and

$$\Delta = \frac{M_3}{M_2} = \frac{h_{31} + R_1h_{32} + R_2h_{33}}{h_{21} + R_1h_{22} + R_2h_{23}} . \qquad (7A2)$$

$$\text{Now} \qquad I_A = \left(\sum_{i=1}^{3} k_{1i}M_i\right) / \eta V \qquad (8A2)$$

So, from eqn. (1A2),

$$\sigma_A^2 = \left[\sum_{i=1}^{3} k_{1i}^2\sigma_{M_i}^2\right] / (\eta V)^2 \qquad (9A2)$$

To find MMCA we solve MMCA = I_A such that

$$\frac{\sigma_A}{I_A} = \frac{1}{\eta V}\,\frac{\left[\sum_{i=1}^{3} (k_{1i})^2\sigma_{M_i}^2\right]^{1/2}}{I_A} = 0.2 \qquad (10A2)$$

Similar expressions are obtained for MMCB and MMCC. We solve for σ_{M_i} given that M_i is a function of the D_i's.

$$\sigma_{M_i}^2 = \sum_{j=1}^{4} \left[\frac{\partial M_i}{\partial D_j}\right]^2 \sigma_{D_j}^2 = \sum_{j=1}^{4} \left[\frac{\partial M_i}{\partial D_j}\right]^2 D_j \qquad (11A2)$$

The partial derivatives are solved to obtain [eqn. (12A2)]

$$\frac{\partial M_1}{\partial D_1} = 1 + s\,w \qquad \frac{\partial M_2}{\partial D_1} = -s\,w \qquad \frac{\partial M_3}{\partial D_1} = -\Delta\, s\, w$$

$$\frac{\partial M_1}{\partial D_2} = -w \qquad \frac{\partial M_2}{\partial D_2} = 1 + \theta + \theta\, s\, w \qquad \frac{\partial M_3}{\partial D_2} = \Delta\, s\, \theta\, w$$

$$\frac{\partial M_1}{\partial D_3} = -\theta\,(1 + s\,w) \qquad \frac{\partial M_2}{\partial D_3} = w \qquad \frac{\partial M_3}{\partial D_3} = \Delta\, w$$

$$\frac{\partial M_1}{\partial D_4} = \theta\, w \qquad \frac{\partial M_2}{\partial D_4} = -\theta\, w \qquad \frac{\partial M_3}{\partial D_4} = 1 + \theta - \Delta\, \theta\, w$$

Substituting (5A2) and (12A2) into (11A2) we find

$$\sigma_{\underline{M}}^2 = N \cdot \underline{M} \qquad (13A2)$$

Where $\sigma_{\underline{M}}^2 = (\sigma_{M_1}^2, \sigma_{M_2}^2, \sigma_{M_2}^2)$
and N is a 3 x 3 matrix with elements

$$n_{11} = (1 + s\,w)^2 + s\,w^2$$

$$n_{12} = \theta(1 + s\,w)^2 \qquad (14A2)$$

$$n_{13} = \theta\, w^2$$

$$n_{21} = s\ (\ s + 1)w^2$$

$$n_{22} = s^2\ w^2 \left[\frac{\theta}{1+\theta}\right] + (1 + \theta + \theta\ s\ w)^2 \left[\frac{1}{1+\theta}\right]$$

$$n_{23} = \theta\ w^2$$

$$n_{31} = \Delta^2\ w^2\ s\ (s + 1)$$

$$n_{32} = \theta(\Delta\ w\ s\ )^2$$

$$n_{33} = \frac{1}{1+\theta}(\ \theta\ \Delta^2\ w^2 + (1 + \theta - \Delta\ w\ \theta)^2)$$

From Section 3.2.2 we have

$$\underline{M} = V\ (H' \cdot \underline{I})\ . \qquad (4)$$

If all the radioactive decays measured are detected with equal efficiency, the matrix H′ can be written as ηH, and thus

$$\underline{M} = \eta V\ (H \cdot \underline{I}),$$

or, written in terms of the vector $\underline{R}$, we have

$$\underline{M} = \eta V\ I_A\ H \cdot \underline{R} = \eta V \frac{I_B}{R_1} H \cdot \underline{R} = \eta V \frac{I_C}{R_2} H \cdot \underline{R} \qquad (15A2)$$

substituting (15A2) and (13A2) into (10A2) we have

$$\frac{\sigma_A}{I_A} = \frac{1}{\eta V}\left[\frac{\sum_{i=1}^{3} (k_{1i})^2\, \eta V(MMCA)\ (N \cdot (H \cdot \underline{R}))_i}{(MMCA)^2}\right]^{1/2} = 0.2$$

(16A2)

with similar expressions for $\frac{\sigma_B}{I_B}$ and $\frac{\sigma_C}{I_C}$.

Solving these equations for MMC's one obtains

$$MMCA = \frac{25}{\eta V}\left[\sum_{i=1}^{3} (k_{1i})^2 \left[N \cdot (H \cdot R)\right]_i\right]$$

$$MMCB = \frac{25}{\eta V} R_1 \left[\sum_{i=1}^{3} (k_{2i})^2 \left[N \cdot (H \cdot R)\right]_i\right] \qquad (17A2)$$

$$MMCC = \frac{25}{\eta V} R_2 \left[\sum_{i=1}^{3} (k_{3i})^2 \left[N \cdot (H \cdot R)\right]_i\right] \ .$$

For the PAEC we have the expression

$$PAEC = \frac{1}{\eta V}\, \underline{L} \cdot \underline{M} \qquad \text{where } \underline{L} = \underline{X} \cdot K \qquad (18A2)$$

$$\text{and } \underline{X} = (0.00103,\ 0.00507,\ 0.00373)$$

Using an analysis similar to that above we obtain

$$MMCWL = \frac{25}{\eta V}\, (\underline{X} \cdot \underline{R}) \left[\sum_{i=1}^{3} l_1^2 [N \cdot (H \cdot \underline{R})]_1\right] \qquad (19A2)$$

Cliff-James-Strong Monitor (CJSM)

The CJSM has three count intervals, counting total alpha decays during sampling and for two time intervals following sampling. The net count vector $\underline{M}$ and raw count vector $\underline{D}$ are equal

$M_1 = D_1$ = alpha counts during sampling,

$M_2 = D_2$ = alpha counts during the first post-sampling count interval

$M_3 = D_3$ = alpha counts during the second post-sampling count interval.

Since the $\underline{M}$ and $\underline{D}$ vectors are identical, the N matrix elements (equation 13A2) are given by

$$n_{ij} = \delta_{ij},$$

where $\delta_{ij} = 1$ for $i = j$

and $\delta_{ij} = 0$ for $i \neq j$.

Given this matrix, equations (17A2) and (19A2) can be used to compute the MMC's for the CJSM.

Environmental Working Level Monitor (EWLM)

Calculation of MMC's for the EWLM must be approached somewhat differently than for the RRDM because θ is not calculated for each sample. Based on data in Keefe, et.al., I assign a value of 0.2 with a standard deviation 0.02 to θ for the EWLM.[16] The raw-counts vector, $\underline{D}$, has elements:

D_1 = alpha counts in low energy channel

D_2 = alpha counts in high energy channel

D_3 = beta counts

The EWLM has a single counting interval.

The corrected counts vector, $\underline{M}$, has elements:

$$M_1 = D_1 - D_2\theta$$
$$M_2 = D_2\ (1 + \theta) \qquad (20A2)$$

$$M_3 = D_3$$

The equations are inverted to obtain

$$D_1 = M_1 + M_2 \left[\frac{\theta}{1 + \theta}\right]$$

$$D_2 = \frac{M_2}{1 + \theta} \qquad (21A2)$$

$$D_3 = M_3$$

We treat M_1 as a function of D_1, D_2, D_3 and θ. Applying equation (1A2) obtains

$$\sigma_{M_1}^2 = M_1 + \theta\, M_2 + \frac{\sigma_\theta^2\, M_2^2}{(1 + \theta)^2}$$

$$\sigma_{M_2}^2 = M_2\ (1 + \theta) + \frac{\sigma_\theta^2\, M_2^2}{(1 + \theta)^2} \qquad (22A2)$$

$$\sigma_{M_3}^2 = M_3$$

These equations can not be written in the form of (13A2), however (22A2) and (15A2) can be used to solve (10A2) and obtain the results [eqn. (23A2)]

$$MMCA = \left[\frac{1}{\eta V}\right] \left[\frac{\sum_{i=1}^{3} (k_{1i})^2 [N \cdot (H \cdot R)]_i}{(0.2)^2 - (\frac{\sigma_\theta}{1+\theta})^2 (h_{21} + h_{22}R_1 + h_{23}R_2)^2 (k_{11}^2 + k_{12}^2)}\right]$$

$$MMCB = \left[\frac{1}{\eta V}\right] \left[\frac{\sum_{i=1}^{3} (k_{2i})^2 [N \cdot (H \cdot R)]_i}{(0.2)^2 - (\frac{\sigma_\theta}{1+\theta})^2 (h_{21} + h_{22}R_1 + h_{23}R_2)^2 (\frac{1}{R_1})^2 (k_{21}^2 + k_{22}^2)}\right]$$

$$MMCC = \left[\frac{1}{\eta V}\right] \left[\frac{\sum_{i=1}^{3} (k_{3i})^2 [N \cdot (H \cdot R)]_i}{(0.2)^2 - (\frac{\sigma_\theta}{1+\theta})^2 (h_{21} + h_{22}R_1 + h_{23}R_2)^2 (\frac{1}{R_2})^2 (k_{31}^2 + k_{32}^2)}\right]$$

where the elements of N are

$n_{11} = 1.0$	$n_{21} = 0$	$n_{31} = 0$
$n_{12} = \theta$	$n_{22} = 1 + \theta$	$n_{32} = 0$
$n_{13} = 0$	$n_{23} = 0$	$n_{33} = 1$

The minimum measurable working level is then [eqn. (24A2)]

$$\text{MMCWL} = \left[\frac{1}{\eta V}\right] \left[\frac{\sum_{i=1}^{3} (l_i)^2 \, [N \cdot (H \cdot R)]_i}{(0.2)^2 - (\frac{\sigma_\theta}{1+\theta})^2 \, (h_{21} + h_{22}R_1 + h_{23}R_2)^2 (\frac{1}{\underline{X} \cdot \underline{R}})^2 (l_1^2 + l_2^2)}\right] .$$

Appendix III. Fortran Program for RRDM Sensitivity Analysis and Optimization

```
      PROGRAM RDMSENS(INPUT,OUTPUT)

C       VERSION 3.3 JANUARY 10, 1980   WILLIAM NAZAROFF
C       INTRODUCTION
C       THIS PROGRAM IS USED TO OPTIMIZE THE TIMING OF VARIOUS RADON
C       DAUGHTER MONITORS.  THE MAIN PROGRAM, ENTITLED 'USER INPUT' IS
C       REWRITTEN FOR EACH OF THE MONITOR SCHEMES.  USUAL OPERATION
C       REQUIRES THE SAMPLING TIME (T0) AND THE TOTAL MEASUREMENT TIME
C       (T1,T2,T3 FOR 1,2, OR 3 COUNT INTERVAL METHODS) TO BE SPECIFIED
C       SUBROUTINES ARE USED TO COMPUTE THE DECAYS OF EACH DAUGHTER
C       DURING OR AFTER SAMPLING, TO INVERT THE MATRIX WHICH CONVERTS
C       ACTIVITY TO COUNTS (H), TO COMPUTE THE MINIMUM MEASURABLE
C       CONCENTRATION FOR EACH DAUGHTER, FOR AN AVERAGE, AND FOR THE
C       PAEC, AND TO CHECK ANY OF THESE VALUES AGAINST THOSE OF THE
C       CURRENT BEST TIMING.

C                          TABLE OF SYMBOLS

C       E AND F TAKE ON VALUES 1,2, OR 3 AND
C       P AND Q TAKE ON THE VALUES A,B, OR C WHERE
C               1=A=RAA=PO-218
C               2=B=RAB=PB-214
C               3=C=RAC=BI-214

C      ALPHA  RATIO OF PO-218 DECAYS IN TIME INTERVAL 2 TO PO-218
C             DECAYS IN TIME INTERVAL 1.
C      B....  BEST VALUE FOR VARIABLE REPRESENTED BY FOLLOWING LETTERS:
C             E.G. BT1 IS THE VALUE OF T1 FOR OPTIMAL SENSITIVITY.
C      DELTA  RATIO OF NET CORRECTED COUNTS IN THIRD MEASUREMENT TO
C             NET CORRECTED COUNTS IN SECOND MEASUREMENT.  USED IN MMC
C             CALCULATION
C      GAMMA  DEFINED AS 1./(DELTA-ALPHA). USED IN MMC CALCULATION.
C      GPQA   DECAYS OF RAP ON THE FILTER DURING THE TIME INTERVAL
C             (T0,T)  (AFTER SAMPLING) DUE TO THE DEPOSITION OF RAQ ON
C             THE FILTER
C      HEF    ELEMENTS OF A 3X3 MATRIX USED TO CONVERT THE AIRBORNE
C             ACTIVITY VECTOR (RAA,RAB,RAC) TO A DECAY VECTOR.
C      KEF    K IS THE INVERSE OF H
C      LP     THE DECAY CONSTANT OF RAP IN UNITS OF MINUTES**-1
C      MMCP   CONCENTRATION OF RAP (UNDER GIVEN CONDITIONS OF R1,R2 AND
C             ASSUMING FLOW RATE*EFFICIENCY=1.0) AT WHICH STATISTICAL
C             UNCERTAINTY IN THE MEASUREMENT IS 20 PER CENT OF THE
C             CONCENTRATION.
C      MMCWL  SAME AS ABOVE FOR WORKING LEVEL
C      MMCS   'AVERAGE' OF MMCP VALUES. COMPUTED BY AVERAGING MMCP
C             WEIGHTED BY 100*WL PER NCI/M**3 OF RAP.
C      NEF    ELEMENTS OF MATRIX M WHICH MULTIPLIES NET COUNT VECTOR
C             TO GIVE VARIANCE ELEMENTS OF NET COUNT VECTOR.
C      R1     RATIO OF PB-214 TO PO-218 ACTIVITIES IN AIR.
C      R2     RATIO OF BI-214 TO PO-218 ACTIVITIES IN AIR.
C      T0     SAMPLING TIME
C      TX     TIME OF BEGINNING OF FIRST COUNT INTERVAL
C      T1     TIME OF END OF FIRST COUNT INTERVAL
C      TY     TIME OF BEGINNING OF SECOND COUNT INTERVAL
C      T2     TIME OF END OF SECOND COUNT INTERVAL
C      TZ     TIME OF BEGINNING OF THIRD COUNT INTERVAL
C      T3     TIME OF END OF THIRD COUNT INTERVAL
C      ALL TIMES ARE IN MINUTES AND ARE REFERENCED TO THE BEGINNING OF
C      SAMPLING.
C      THETA  OVERLAP FACTOR - COUNTS IN RAA PEAK DUE TO RAC DECAYS
```

```
C              DIVIDED BY COUNTS IN RAC PEAK DUE TO RAC DECAYS.

C         INITIALIZATION
      IMPLICIT REAL(H,K,L,M,N)
      DIMENSION R1(6),R2(5)
      COMMON GAAD,GBAD,GB6D,GCAD,GC8D,GCCD,GAAA,GBAA,GBBA,GCAA,GCBA,GCCA
     R,T0,LA,LB,LC,H11,H12,H13,H21,H22,H23,H31,H32,H33,K11,K12,K13,K21,K
     R22,K23,K31,K32,K33,MMCA,MMCB,MMCC,MMCWL,MMCS,BMMCS,BMMCA,BMMCB,BMM
     RCC,BMMCWL,X1,X2,X3,N11,N12,N13,N21,N22,N23,N31,N32,N33,BK11,BK12,B
     RK13,BK21,BK22,BK23,BK31,BK32,BK33
      LA=0.227261
      LB=0.025864
      LC=0.035185
      DATA (R1(J),J=1,6)/1.0,0.9,0.6,0.4,0.3,0.1/
      DATA (R2(J),J=1,6)/1.0,0.75,0.4,0.25,0.1,0.02/
      X1=0.00103
      X2=0.00507
      X3=0.00373

C         USER INPUT

C         RESIDENTIAL RADON DAUGHTER MONITOR
C         THIS PROGRAM TAKES AS INPUT THE SAMPLING TIME AND TOTAL MEAS-
C         UREMENT TIME AND CALCULATES THE BEST INTERMEDIATE TIMING SCHEME
C         FOR THE RESIDENTIAL RADON DAUGHTER MONITOR (RRDM).  THE RRDM
C         USES 2 CHANNEL ALPHA SPECTROSCOPY AND TWO COUNTING INTERVALS
C         AFTER SAMPLING.

C         DEFINE OVERLAP
      THETA=0.05
      WRITE 5,THETA

C         READ INPUT
  100 READ 15,T0,T2
      IF (T0.EQ.0.0) GO TO 999
      TX=T0+1.0

C         DECAYS UP TO TX AND T2
      CALL AFTER (TX)
      AAAX=GAAA
      CAAX=GCAA
      CBAX=GCBA
      CCAX=GCCA

      CALL AFTER (T2)
      CAA2=GCAA
      CBA2=GCBA
      CCA2=GCCA

      JT0=T0
      JT2=T2

C         LOOP FOR EACH DISEQUILIBRIUM CONDITION
      DO 250 I=1,6
      BMMCS=1000.0

C         ON FIRST PASS LOOK AT EVERY FOURTH MINUTE FOR TY AND T2
      JPASS=1
      JSTEP=4

      JT1MIN=JT0+2
      JT1MAX=JT2-2
```

```
  110 DO 200 JT1=JT1MIN,JT1MAX,JSTEP
      T1=1.0*JT1

C         COMPUTE DECAYS DURING FIRST TIME INTERVAL
      CALL AFTER (T1)
      AAA1=GAAA-AAAX
      CAA1=GCAA-CAAX
      CBA1=GCBA-CBAX
      CCA1=GCCA-CCAX

      JTYMIN=JT1+1
      JTYMAX=JT2-1
      DO 200 JTY=JTYMIN,JTYMAX,JSTEP
      TY=1.0*JTY

C         COMPUTE DECAYS DURING SECOND TIME INTERVAL
      CALL AFTER (TY)

C         COMPUTE ELEMENTS OF H MATRIX
      H11=AAA1
      H12=0.0
      H13=0.0
      H21=CAA1
      H22=CBA1
      H23=CCA1
      H31=CAA2-GCAA
      H32=CBA2-GCBA
      H33=CCA2-GCCA

C         COMPUTE ELEMENTS OF K MATRIX
      CALL INVERT (DUMMY)

C         COMPUTE ELEMENTS OF VARIANCE CONVERSION MATRIX N
      Z1=H21*R1(I)*H22*R2(I)*H23
      Z2=H31*R1(I)*H32*R2(I)*H33
      ALPHA=(EXP(-LA*TY)-EXP(-LA*T2))/(EXP(-LA*TX)-EXP(-LA*T1))
      GAMMA=Z1/(Z2-ALPHA*Z1)
      DELTA=Z2/Z1

      N11=(1.0+ALPHA*GAMMA)**2+ALPHA*GAMMA**2
      N12=THETA*(1.0+ALPHA*GAMMA)**2
      N13=THETA*GAMMA**2
      N21=ALPHA*(1.0+ALPHA)*GAMMA**2
      N22=(ALPHA*GAMMA)**2*(THETA/(1.0+THETA))+(1.0+THETA*(1.0+ALPHA*GAM
     RMA))**2/(1.0+THETA)
      N23=THETA*GAMMA**2
      N31=ALPHA*(1.0+ALPHA)*(DELTA*GAMMA)**2
      N32=THETA*(DELTA*GAMMA*ALPHA)**2
      N33=(THETA*(DELTA*GAMMA)**2+(1.0+THETA-DELTA*GAMMA*THETA)**2)/(1.0
     R+THETA)

C         SOLVE FOR MINIMUM MEASURABLE CONCENTRATIONS
      CALL MINSENS (R1(I),R2(I),I)

C         IS THIS THE BEST SO FAR
      CALL BEST (T1,TY,BT1,BTY)
  200 CONTINUE
C         DO TWO PASSES THROUGH
      IF (JPASS.EQ.2) GO TO 225
      JPASS=2
      JSTEP=1
```

```
C         SET NARROW LIMITS FOR SECOND PASS SEARCH
      IF (BT1-4.0.GT.1.0*JT1MIN) JT1MIN=BT1-4.0
      IF (BT1+4.0.LT.1.0*JT1MAX) JT1MAX=BT1+4.0
      IF (BTY+5.0.LT.1.0*JT2) JT2=BTY+5.0
      GO TO 110
(
C         OUTPUT
  225 WRITE 20,R1(I),R2(I)
      WRITE 30
      WRITE 40,T0,TX,BT1,BTY,T2,BMMCA,BMMCB,BMMCC,BMMCWL,BMMCS
      WRITE 50
      WRITE 60,BK11,BK12,BK13,BK21,BK22,BK23,BK31,BK32,BK33

  250 CONTINUE

      GO TO 100

    5 FORMAT (1H1,*    RESIDENTIAL RADON DAUGHTER MONITOR OPTIMIZATION*/
     R*       THETA=*,F4.2)
   15 FORMAT (2F5.1)
   20 FORMAT (//20X,*R1?R2 =*,F4.2,*?*,F4.2/)
   30 FORMAT (*   T0   TX   T1   TY   T2         MMCA     MMCB     MMCC     MMCW
     RL     MMCS*)
   40 FORMAT (2X,5F4.0,4X,3F8.3,F9.6,F8.3)
   50 FORMAT (/*     K11      K12      K13      K21      K22      K23      K31
     R     K32      K33*)
   60 FORMAT (1X,9F8.6//)

  999 END
```

```
C       DECAY COEFFICIENTS *DURING* SAMPLING

C       THIS SUBROUTINE TAKES AS INPUT T, THEN COMPUTES THE DECAYS
C       FROM 0 TO T ON THE FILTER DURING SAMPLING OF EACH DAUGHTER DUE
C       TO THE DEPOSITION OF THE DAUGHTER AND THOSE ABOVE IT IN THE
C       DECAY CHAIN.

      SUBROUTINE DURING (T)

      IMPLICIT REAL(M,K,L,N)
      COMMON GAAD,GBAD,GBBD,GCAD,GCBD,GCCD,GAAA,GBAA,GBBA,GCAA,GCBA,GCCA
     R,T0,LA,LB,LC,M11,M12,M13,M21,M22,M23,M31,M32,M33,K11,K12,K13,K21,K
     R22,K23,K31,K32,K33,MMCA,MMCB,MMCC,MMCWL,MMCS,BMMCS,BMMCA,BMMCB,BMM
     RCC,BMMCWL,X1,X2,X3,N11,N12,N13,N21,N22,N23,N31,N32,N33,BK11,BK12,B
     RK13,BK21,BK22,BK23,BK31,BK32,BK33

      GAAD=(T-(1./LA)*(1.-EXP(-LA*T)))/LA**2.22
      GBAD=(T-LB*(1.-EXP(-LA*T))/LA/(LB-LA)-LA*(1.-EXP(-LB*T))/LB/(LA-LB
     R))/LA**2.22
      GBBD=(T-(1./LB)*(1.-EXP(-LB*T)))/LB**2.22
      GCAD=(T-LB*LC*(1.-EXP(-LA*T))/LA/(LB-LA)/(LC-LA)-LA*LC*(1.-EXP(-LB
     R*T))/LB/(LA-LB)/(LC-LB)-LA*LB*(1.-EXP(-LC*T))/LC/(LB-LC)/(LA-LC))/
     RLA**2.22
      GCBD=(T-LC*(1.-EXP(-LB*T))/LB/(LC-LB)-LB*(1.-EXP(-LC*T))/LC/(LB-LC
     R))/LB**2.22
      GCCD=(T-(1.-EXP(-LC*T))/LC)/LC**2.22

      RETURN
      END
```

```
C       DECAY COEFFICIENTS *AFTER* SAMPLING

C       THIS SUBROUTINE TAKES AS INPUT THE TIME T, THEN COMPUTES THE
C       DECAYS FROM T0 TO T ON THE FILTER OF EACH DAUGHTER DUE TO THE
C       DEPOSITION OF THAT DAUGHTER AND THOSE ABOVE IT IN THE CHAIN.
C       SAMPLING TIME IS ASSUMED TO BE T0.

      SUBROUTINE AFTER (T)

      IMPLICIT REAL(H,K,L,M,N)
      COMMON GAAD,GBAD,GBBD,GCAD,GCBD,GCCD,GAAA,GBAA,GBBA,GCAA,GCBA,GCCA
     R,T0,LA,LB,LC,H11,H12,H13,H21,H22,H23,H31,H32,H33,K11,K12,K13,K21,K
     R22,K23,K31,K32,K33,MMCA,MMCB,MMCC,MMCWL,MMCS,BMMCS,BMMCA,BMMCB,BMM
     RCC,BMMCWL,X1,X2,X3,N11,N12,N13,N21,N22,N23,N31,N32,N33,BK11,BK12,B
     RK13,BK21,BK22,BK23,BK31,BK32,BK33

      GAAA=(1.-EXP(-LA*T0))*(1.-EXP(-LA*(T-T0)))/LA**2*2.22
      GBAA=(LB*(1.-EXP(-LA*(T-T0)))*(1.-EXP(-LA*T0))/LA/(LB-LA)+LA*(1.-E
     RXP(-LB*(T-T0)))*(1.-EXP(-LB*T0))/LB/(LA-LB))/LA*2.22
      GBBA=(1.-EXP(-LB*T0))*(1.-EXP(-LB*(T-T0)))/LB**2*2.22
      GCAA=(LB*LC*(1.-EXP(-LA*(T-T0)))*(1.-EXP(-LA*T0))/LA/(LB-LA)/(LC-L
     RA)+LC*LA*(1.-EXP(-LB*(T-T0)))*(1.-EXP(-LB*T0))/LB/(LA-LB)/(LC-LB)+
     RLA*LB*(1.-EXP(-LC*(T-T0)))*(1.-EXP(-LC*T0))/LC/(LA-LC)/(LB-LC))/LA
     R*2.22
      GCBA=(LC*(1.-EXP(-LB*(T-T0)))*(1.-EXP(-LB*T0))/LB/(LC-LB)+LB*(1.-E
     RXP(-LC*(T-T0)))*(1.-EXP(-LC*T0))/LC/(LB-LC))/LB*2.22
      GCCA=(1.-EXP(-LC*(T-T0)))*(1.-EXP(-LC*T0))/LC**2*2.22

      RETURN
      END
```

```
C         INVERT H MATRIX

C         THIS SUBROUTINE SOLVES FOR THE ELEMENTS OF K WHICH IS THE
C         INVERSE OF THE H MATRIX.

       SUBROUTINE INVERT (DUMMY)

       IMPLICIT REAL(H,K,L,M,N)
       COMMON GAAD,GBAD,GBBD,GCAD,GCBD,GCCD,GAAA,GBAA,GBBA,GCAA,GCBA,GCCA
      R,TD,LA,LB,LC,H11,H12,H13,H21,H22,H23,H31,H32,H33,K11,K12,K13,K21,K
      R22,K23,K31,K32,K33,MMCA,MMCB,MMCC,MMCWL,MMCS,BMMCS,BMMCA,BMMCB,BMM
      RCC,BMMCWL,X1,X2,X3,N11,N12,N13,N21,N22,N23,N31,N32,N33,BK11,BK12,B
      RK13,BK21,BK22,BK23,BK31,BK32,BK33

       DETH=H11*(H22*H33-H32*H23)+H12*(H23*H31-H21*H33)+H13*(H21*H32-H22*
      RH31)
       K11=(H22*H33-H23*H32)/DETH
       K12=-(H12*H33-H32*H13)/DETH
       K13=(H12*H23-H13*H22)/DETH
       K21=-(H21*H33-H23*H31)/DETH
       K22=(H11*H33-H13*H31)/DETH
       K23=-(H11*H23-H13*H21)/DETH
       K31=(H21*H32-H22*H31)/DETH
       K32=-(H11*H32-H12*H31)/DETH
       K33=(H11*H22-H12*H21)/DETH

       RETURN
       END
```

```
C       MINIMUM MEASURABLE CONCENTRATIONS

C       THIS SUBROUTINE COMPUTES THE MINIMUM MEASURABLE CONCENTRATIONS
C       OF RADON DAUGHTERS AND WL.  AT THE MMC THE UNCERTAINTY IN THE
C       MEASUREMENT IS 20 PERCENT.

      SUBROUTINE MINSENS (R1,R2,I)

      IMPLICIT REAL(H,K,L,M,N)
      COMMON GAAD,GBAD,GBBD,GCAD,GC9D,GCCD,GAAA,GBAA,GBBA,GCAA,GC8A,GCCA
     R,T0,LA,LB,LC,H11,H12,H13,H21,H22,H23,H31,H32,H33,K11,K12,K13,K21,K
     R22,K23,K31,K32,K33,MMCA,MMCB,MMCC,MMCWL,MMCS,BMMCS,BMMCA,BMMCB,BMM
     RCC,BMMCWL,X1,X2,X3,N11,N12,N13,N21,N22,N23,N31,N32,N33,BK11,BK12,B
     RK13,BK21,BK22,BK23,BK31,BK32,BK33

      H1R=H11+H12*R1+H13*R2
      H2R=H21+H22*R1+H23*R2
      H3R=H31+H32*R1+H33*R2
      N1HR=N11*H1R+N12*H2R+N13*H3R
      N2HR=N21*H1R+N22*H2R+N23*H3R
      N3HR=N31*H1R+N32*H2R+N33*H3R
      MMCA=25.*(K11**2*N1HR+K12**2*N2HR+K13**2*N3HR)
      MMCB=25.*(K21**2*N1HR+K22**2*N2HR+K23**2*N3HR)/R1
      MMCC=25.*(K31**2*N1HR+K32**2*N2HR+K33**2*N3HR)/R2
      L1=X1*K11+K21*X2+X3*K31
      L2=X1*K12+X2*K22+X3*K32
      L3=X1*K13+X2*K23+X3*K33
      MMCWL=25.*(L1**2*N1HR+L2**2*N2HR+L3**2*N3HR)/(X1+X2*R1+X3*R2)
      MMCS=((MMCA+MMCB/R1+MMCC/R2)/3.0)*(X1+X2*R1+X3*R2)*100.0

      RETURN
      END
```

```
C       SEARCH FOR BEST TIMING

C       THIS SUBROUTINE MAINTAINS A RECORD OF THE BEST TIMING, MMC'S,
C       AND K MATRIX OBSERVED TO THAT POINT IN THE PROGRAM.
      SUBROUTINE BEST (TA,TB,BTA,BTB)

      IMPLICIT REAL(H,K,L,M,N)
      COMMON GAAD,GBAD,GBBD,GCAD,GCBD,GCCD,GAAA,GBAA,GBBA,GCAA,GCBA,GCCA
     R,TO,LA,LB,LC,H11,H12,H13,H21,H22,H23,H31,H32,H33,K11,K12,K13,K21,K
     R22,K23,K31,K32,K33,MMCA,MMCB,MMCC,MMCWL,MMCS,BMMCS,BMMCA,BMMCB,BMM
     RCC,BMMCWL,X1,X2,X3,N11,N12,N13,N21,N22,N23,N31,N32,N33,BK11,BK12,B
     RK13,BK21,BK22,BK23,BK31,BK32,BK33

      IF (BMMCS.LT.MMCS) RETURN
      BMMCS=MMCS
      BTA=TA
      BTB=TB
      BMMCA=MMCA
      BMMCB=MMCB
      BMMCC=MMCC
      BMMCWL=MMCWL
      BK11=K11
      BK12=K12
      BK13=K13
      BK21=K21
      BK22=K22
      BK23=K23
      BK31=K31
      BK32=K32
      BK33=K33

      RETURN
      END
```

List of Figures

Fig. 12. Concentrations of individual radon daughters as a function of time in the energy research house immediately after the furnace fan, which recirculates indoor air, is shut off. The growth of ^{214}Po and ^{214}Bi concentrations are well-fitted by exponential growth curves with time constants equal to the air exchange rate (0.07/hr) rather than the daughter decay constants (2.2 and 3.0/hr). This behavior indicates that while the furnace fan acts as a removal mechanism for these daughters, the action is through an agent, rather than direct.

---

*Notes on Figs. 2-6:

The MMCS is defined by the equation:

$$MMCS = (MMCA + MMCB/R_1 + MMCC/R_2)\ (Q/3)$$

where

$$Q = 0.103 + 0.507\ R_1 + 0.373\ R_2$$

MMCx is the concentration of I_x at which the relative standard deviation in the measurement is 20%, assuming the product of the detector efficiency a sampling flow rate is 1.0 (counts per disintegration-liters per minute).

R_1 and R_2 are the ratios of ^{214}Pb and ^{214}Bi activity, respectively, to the activity of ^{218}Po. $R_1:R_2 = 0.6:0.4$ are taken as typical values. The parameter θ expresses the overlap of the energy peaks, that is the ratio of ^{214}Po alpha disintegrations appearing as counts in the lower level alpha channel to those appearing as counts in the upper level alpha channel.

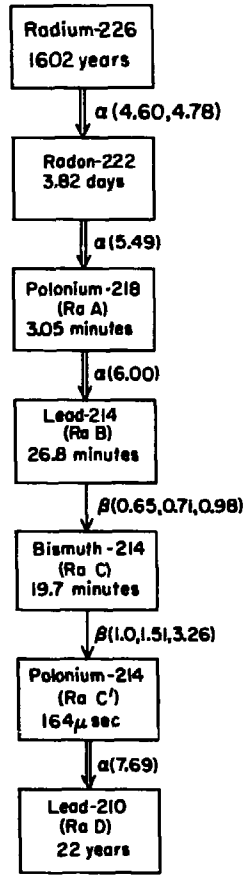
Radium-226
1602 years
α (4.60,4.78)
Radon-222
3.82 days
α(5.49)
Polonium-218
(Ra A)
3.05 minutes
α(6.00)
Lead-214
(Ra B)
26.8 minutes
β(0.65,0.71,0.98)
Bismuth-214
(Ra C)
19.7 minutes
β(1.0,1.51,3.26)
Polonium-214
(Ra C')
164μ sec
α(7.69)
Lead-210
(Ra D)
22 years
XBL7212-4903

Figure 1

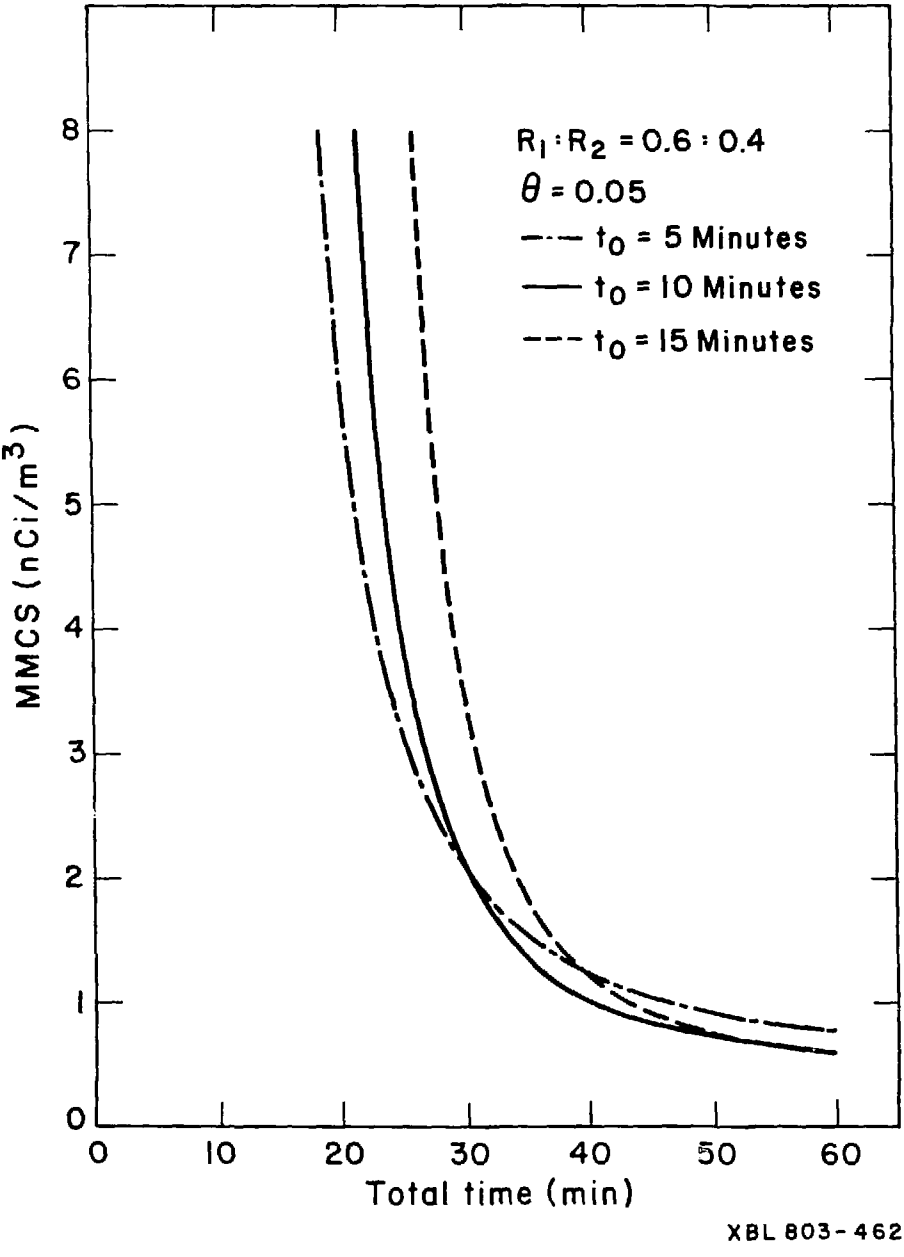
$R_1 : R_2 = 0.6 : 0.4$
$\theta = 0.05$
t_0 = 5 Minutes
t_0 = 10 Minutes
t_0 = 15 Minutes
MMCS (nCi/m^3)
0
1
2
3
4
5
6
7
8
0
10
20
30
40
50
60
Total time (min)
XBL 803-462

Figure 2

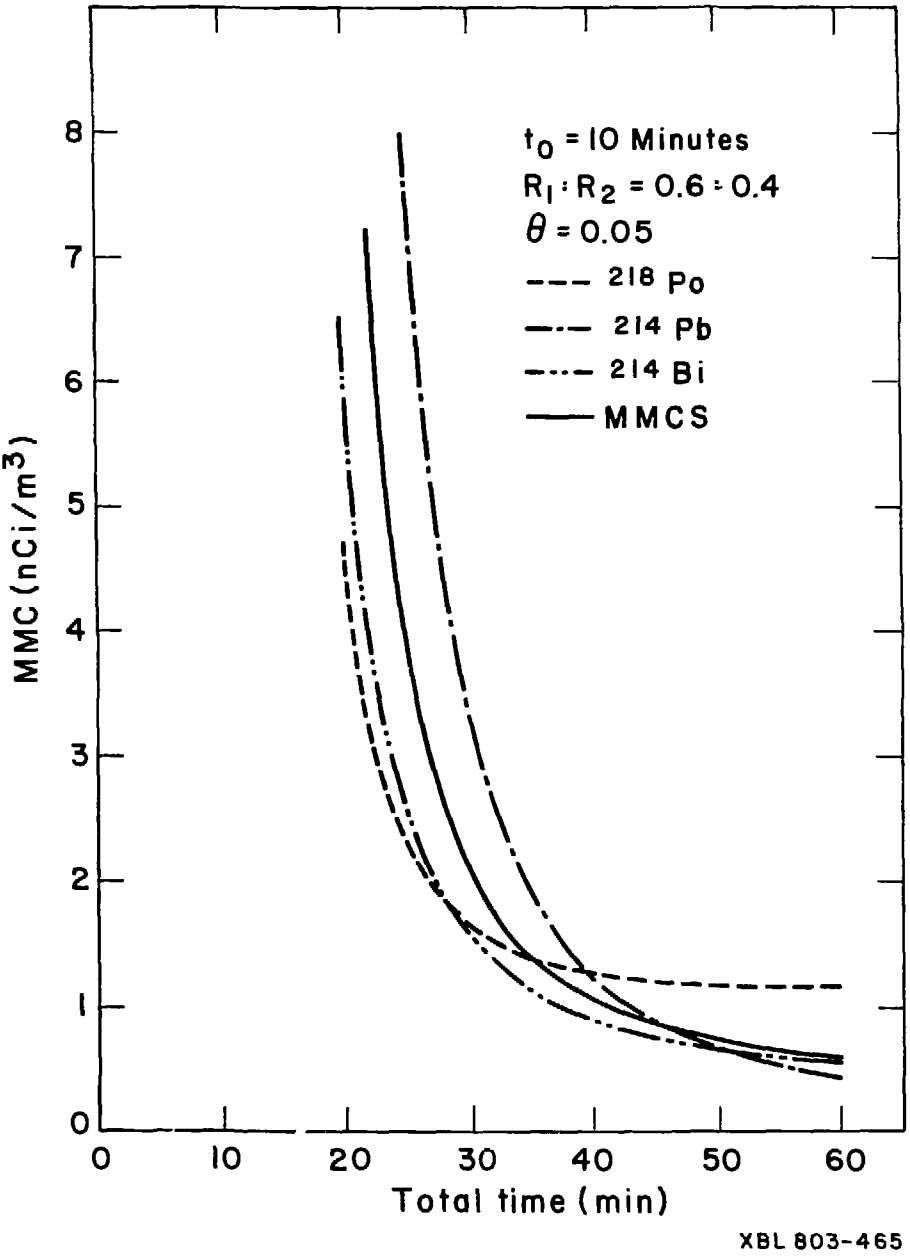
t_0 = 10 Minutes
$R_1 : R_2$ = 0.6 : 0.4
θ = 0.05
218 Po
214 Pb
214 Bi
MMCS
MMC (nCi/m^3)
Total time (min)
0
1
2
3
4
5
6
7
8
0
10
20
30
40
50
60
XBL 803-465

Figure 3

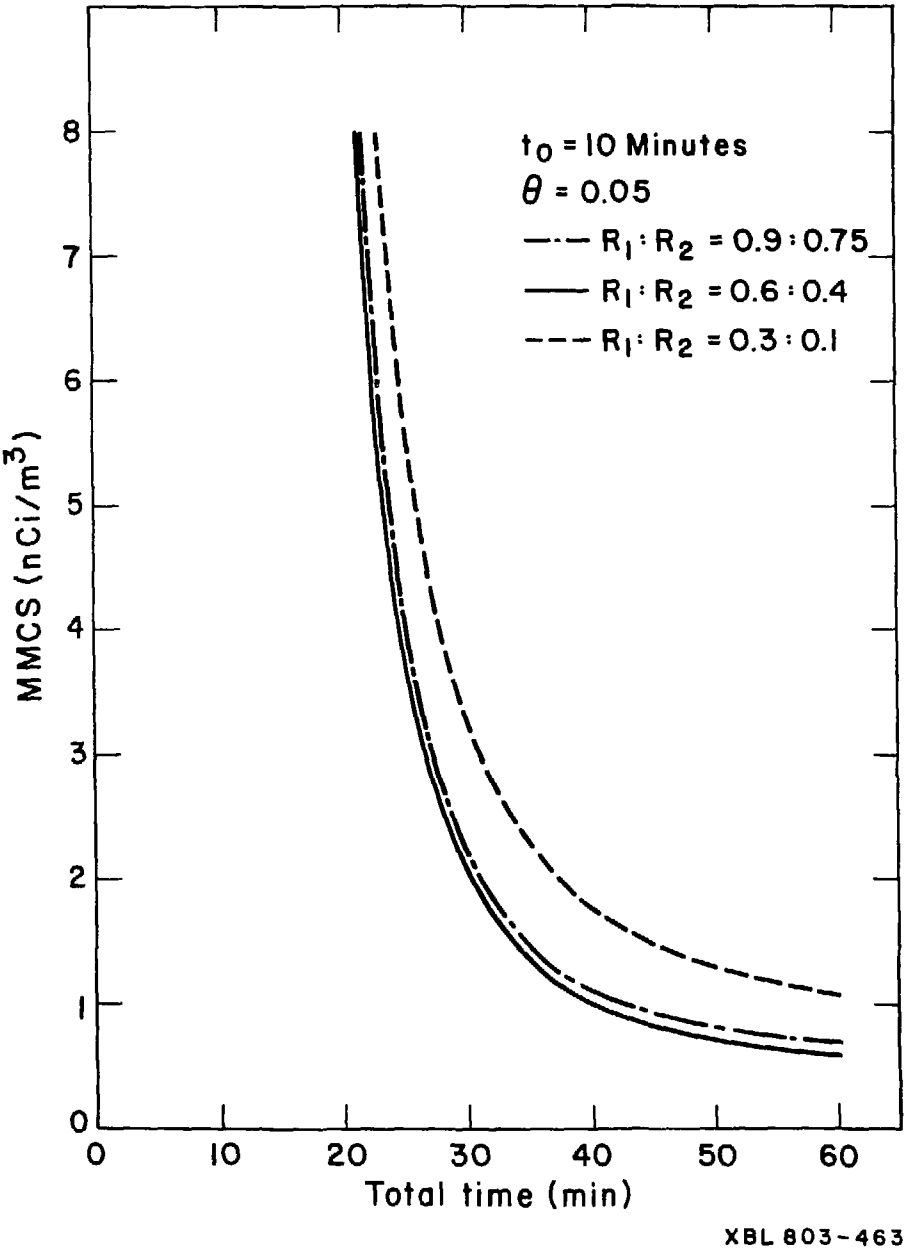
t_0 = 10 Minutes
θ = 0.05
$R_1 : R_2$ = 0.9 : 0.75
$R_1 : R_2$ = 0.6 : 0.4
$R_1 : R_2$ = 0.3 : 0.1
MMCS (nCi/m^3)
Total time (min)
0
1
2
3
4
5
6
7
8
0
10
20
30
40
50
60
XBL 803-463

Figure 4

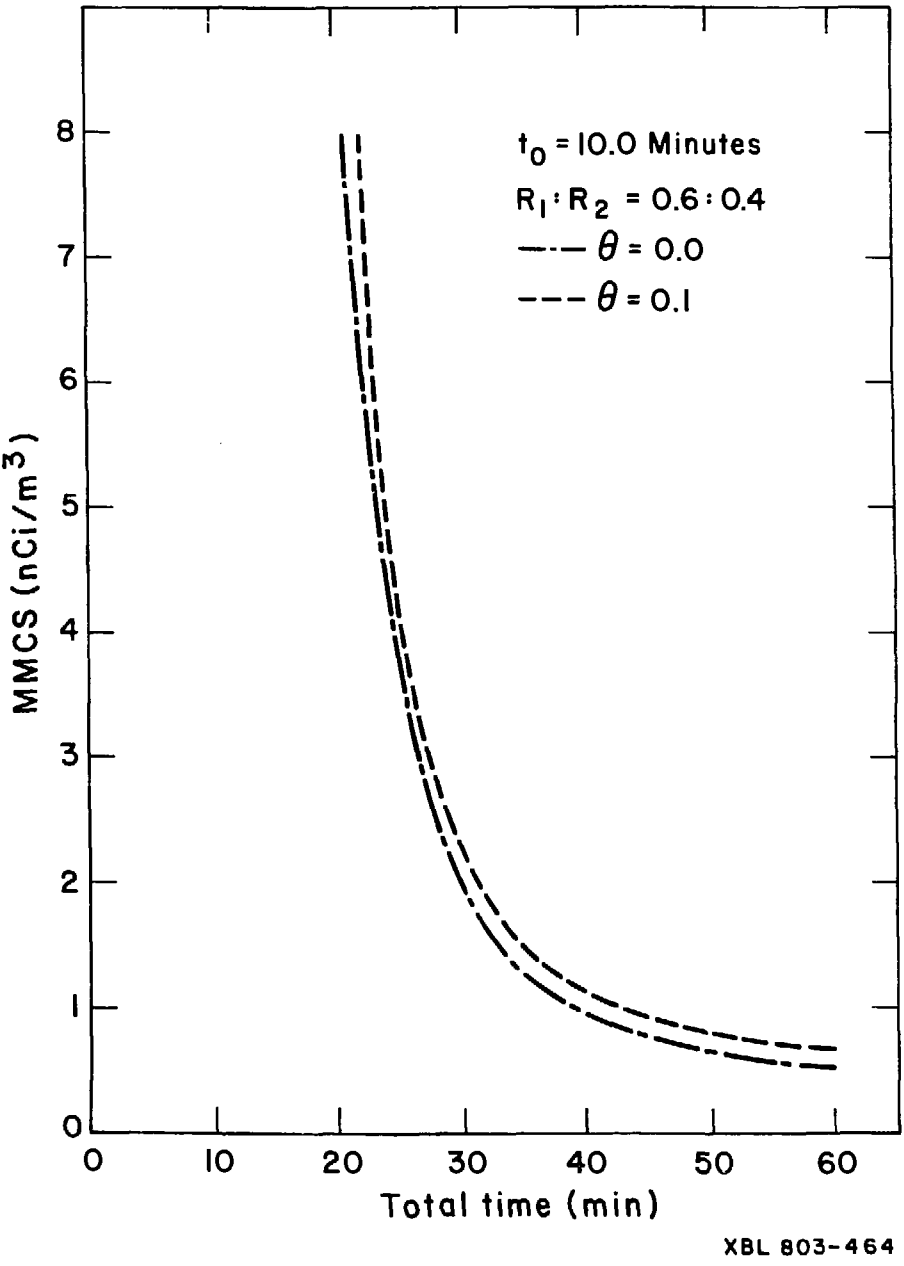
t_0 = 10.0 Minutes
$R_1 : R_2$ = 0.6 : 0.4
— · — θ = 0.0
— — — θ = 0.1
MMCS (nCi/m^3)
0
1
2
3
4
5
6
7
8
0
10
20
30
40
50
60
Total time (min)
XBL 803-464

Figure 5

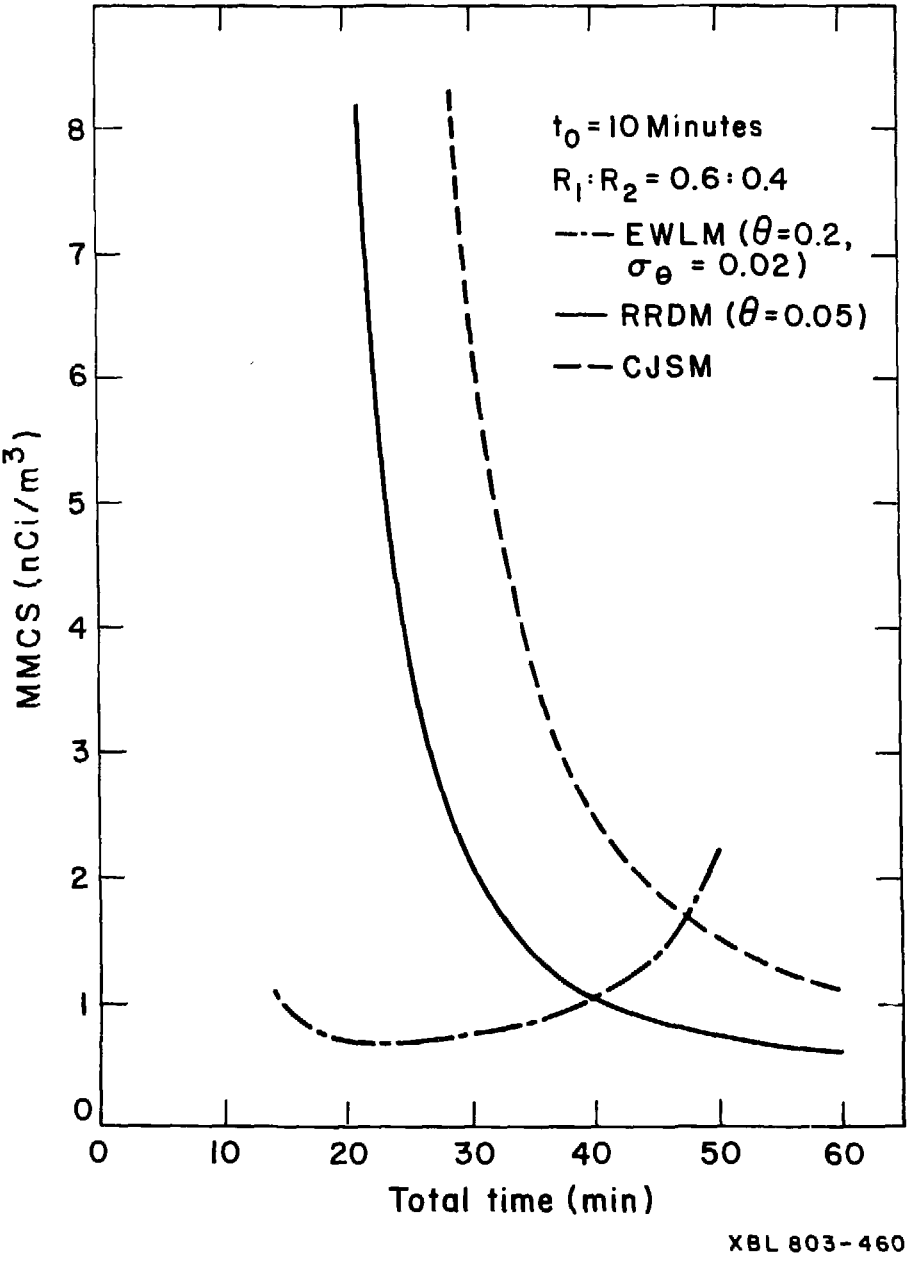
t_0 = 10 Minutes
$R_1 : R_2$ = 0.6 : 0.4
EWLM (θ=0.2, σ_θ = 0.02)
RRDM (θ=0.05)
CJSM
MMCS (nCi/m^3)
Total time (min)
0
10
20
30
40
50
60
1
2
3
4
5
6
7
8
XBL 803-460

Figure 6

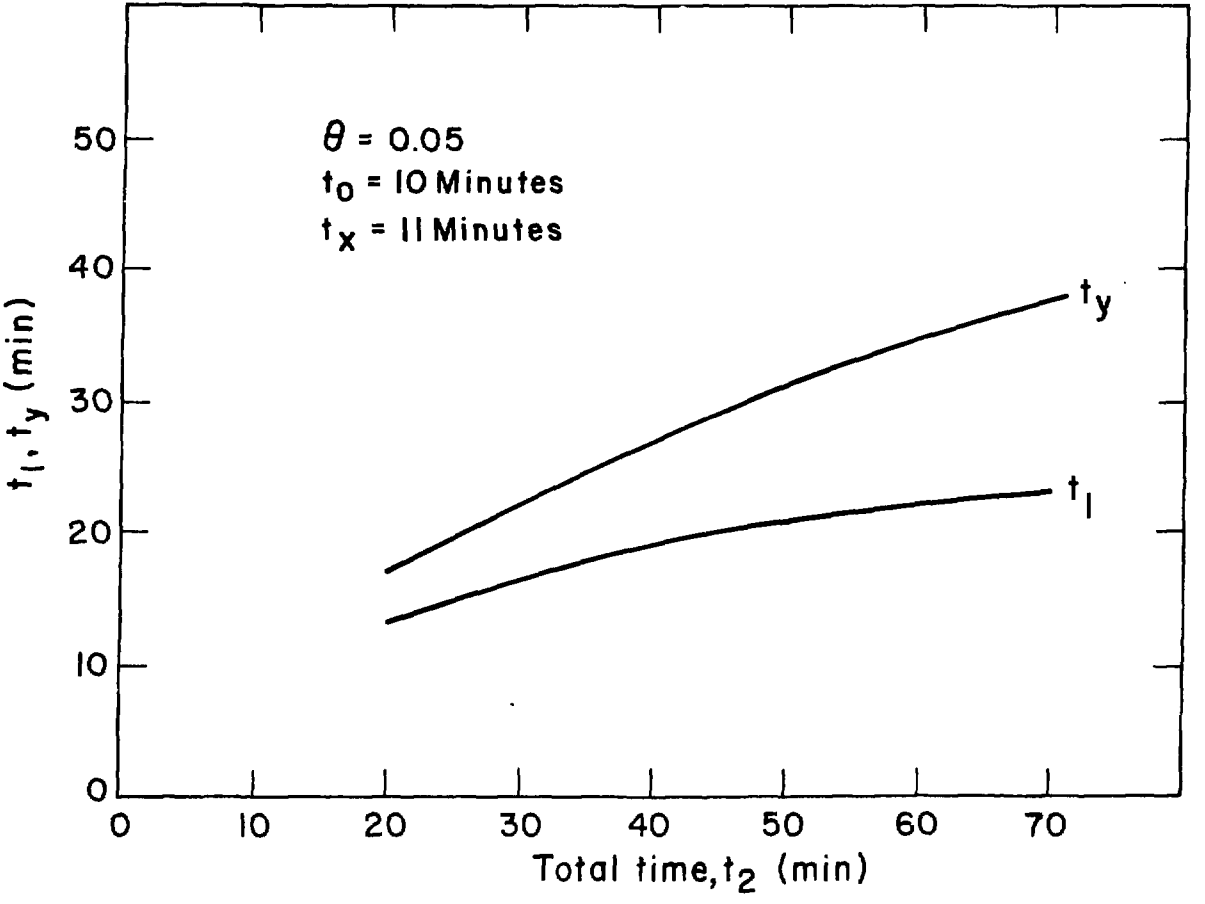
θ = 0.05
t0 = 10 Minutes
tx = 11 Minutes
ty
t1
t1, ty (min)
Total time, t2 (min)
0
10
20
30
40
50
60
70
XBL 803-466

Figure 7

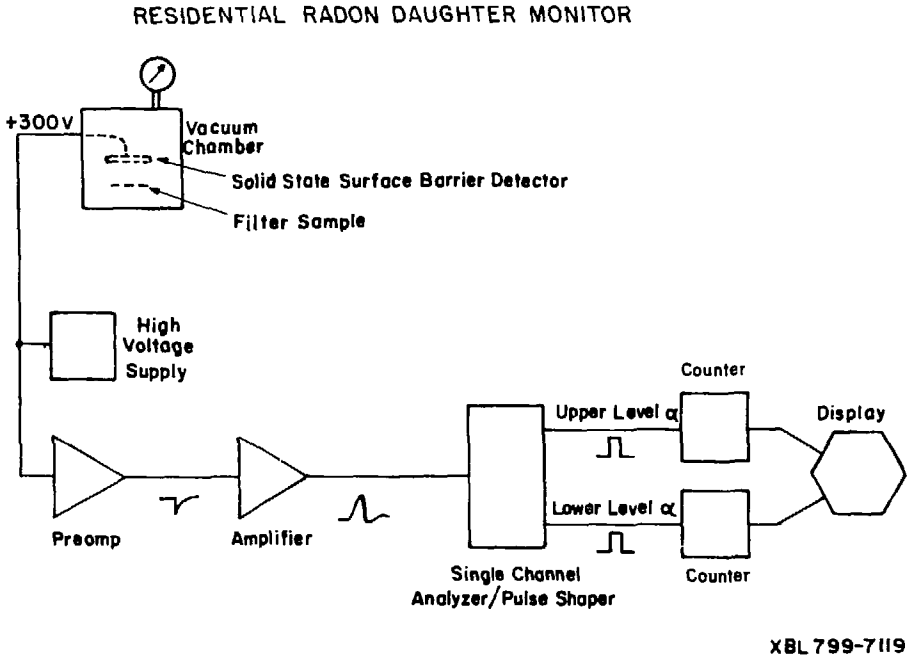
RESIDENTIAL RADON DAUGHTER MONITOR
+300v
Vacuum Chamber
Solid State Surface Barrier Detector
Filter Sample
High Voltage Supply
Counter
Upper Level α
Display
Lower Level α
Preamp
Amplifier
Single Channel Analyzer/Pulse Shaper
Counter
XBL 799-7119

Figure 8

Figure 9

XBB 790-14639

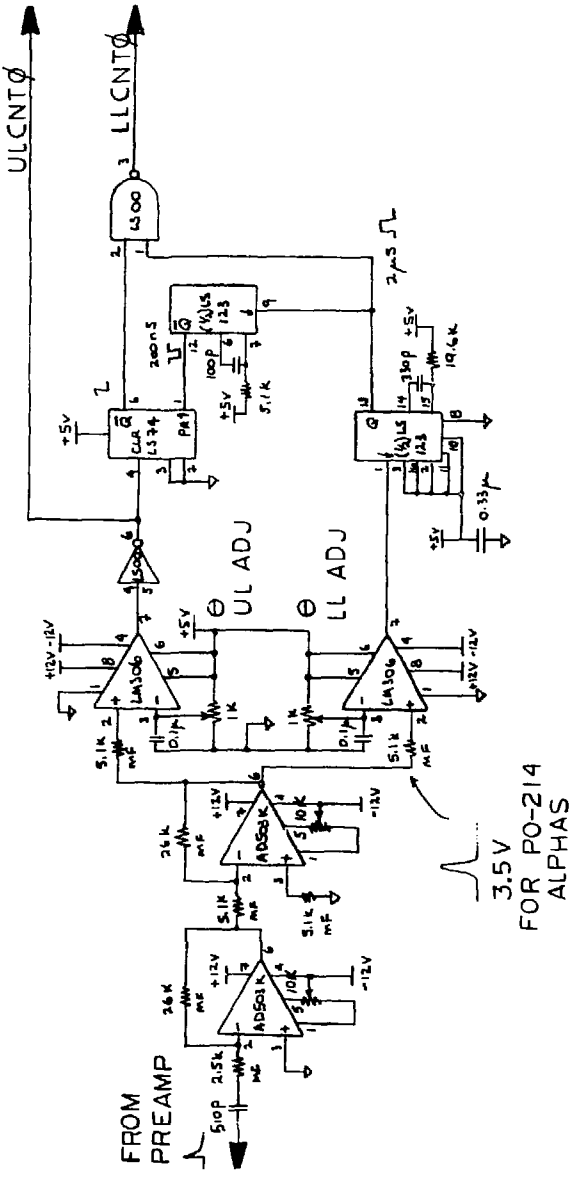

XBL 805-9491

Fig. 10A

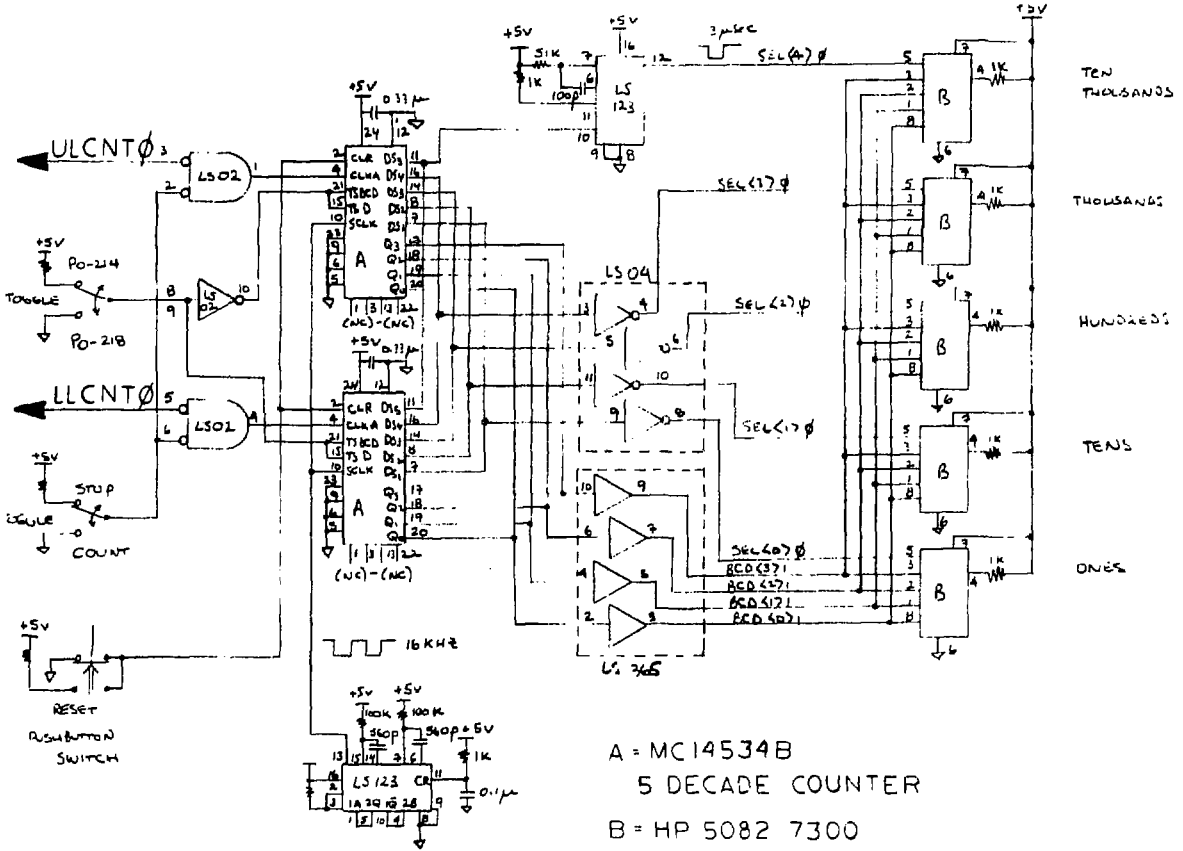
ULCNTØ
LLCNTØ
LS02
LS02
LS04
LS 365
LS 123
LS123
+5V
Po-214
Po-218
TOGGLE
STOP
COUNT
RESET
PUSHBUTTON SWITCH
16KHZ
SEL(4)Ø
SEL(3)Ø
SEL(2)Ø
SEL(1)Ø
SEL(0)Ø
BCD(3)
BCD(2)
BCD(1)
BCD(0)
TEN THOUSANDS
THOUSANDS
HUNDREDS
TENS
ONES
A = MC14534B
5 DECADE COUNTER
B = HP 5082 7300
4X7 DOT MATRIX LATCHING DISPLAY
XBL 805-9492

Fig. 10B

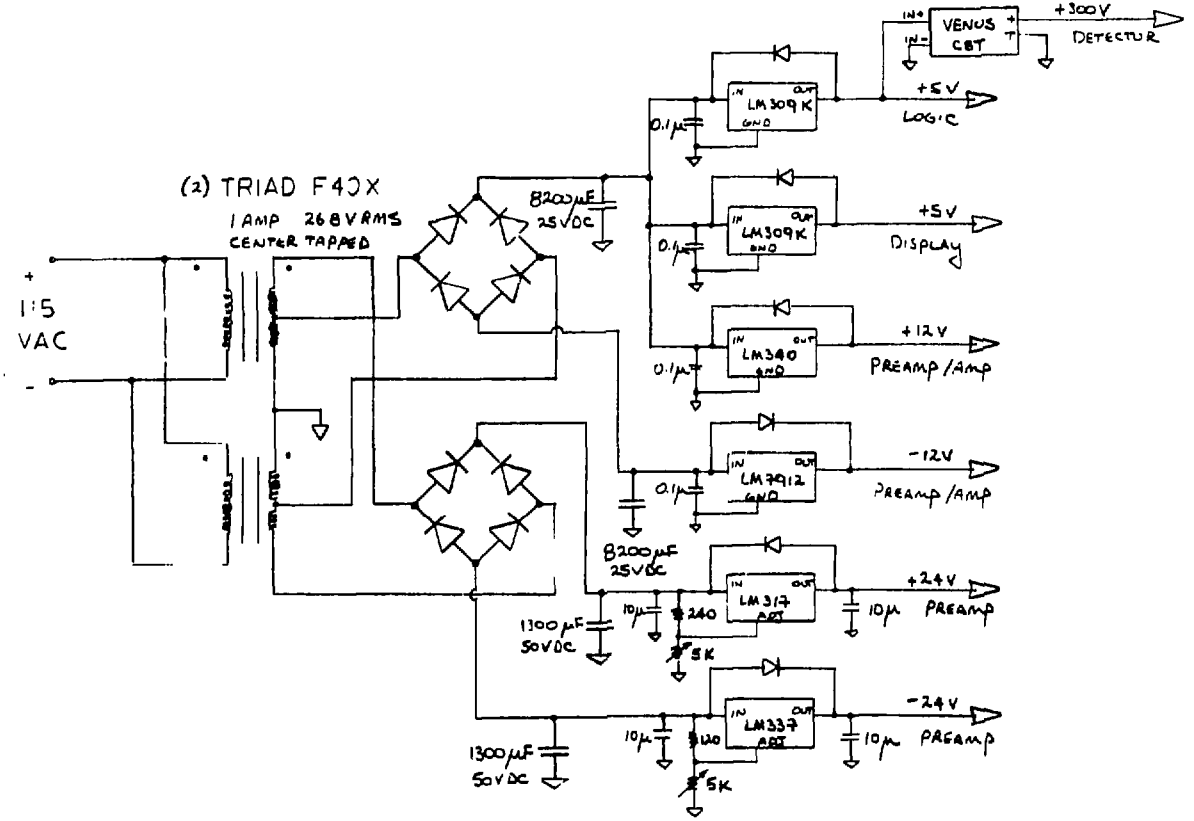

XBL 805-9493

Fig. 10C

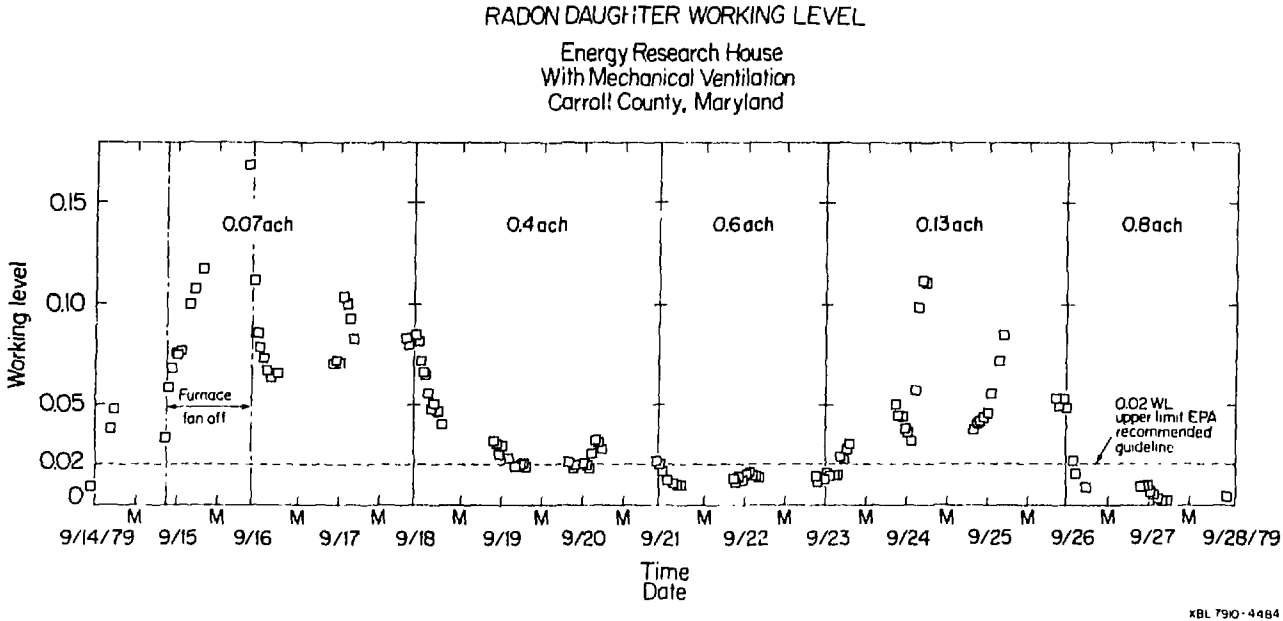
RADON DAUGHTER WORKING LEVEL
Energy Research House
With Mechanical Ventilation
Carroll County, Maryland
Working level
0.15
0.10
0.05
0.02
0
0.07ach
0.4ach
0.6ach
0.13ach
0.8ach
Furnace
fan off
0.02 WL
upper limit EPA
recommended
guideline
M
9/14/79
9/15
9/16
9/17
9/18
9/19
9/20
9/21
9/22
9/23
9/24
9/25
9/26
9/27
9/28/79
Time
Date
XBL 790-4484

Fig. 11

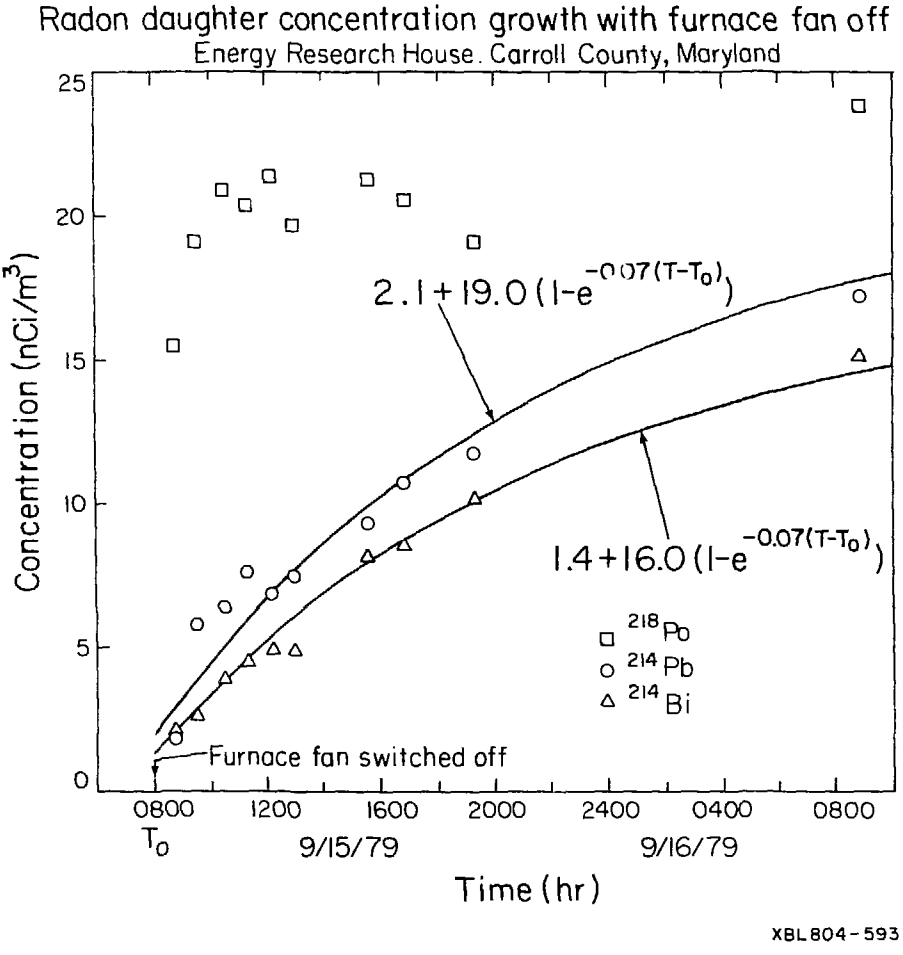
Radon daughter concentration growth with furnace fan off
Energy Research House. Carroll County, Maryland
Concentration (nCi/m3)
25
20
15
10
5
0
2.1+19.0(1-e-0.07(T-T0))
1.4+16.0(1-e-0.07(T-T0))
218Po
214Pb
214Bi
Furnace fan switched off
0800
1200
1600
2000
2400
0400
0800
T0
9/15/79
9/16/79
Time (hr)
XBL804-593

Figure 12

Table 1. Comparison of Minimum Measurable Concentrations of Radon Daughters for Various Sampling Techniques.

Method (t_0,t_x-t_1,t_y-t_2,t_z-t_3) (minutes)	R_1:R_2	MMCA (nCi/m^3)	MMCB (nCi/m^3)	MMCC (nCi/m^3)	MMCWL (WL)	MMCS (nCi/m^3)
Thomas-Tsivoglou	0.9:0.75	56.8	6.2	8.6	0.0100	21.0
(5,7-10,11-25,26-35)	0.6:0.4	37.0	5.9	10.2	0.0096	13.4
	0.3:0.1	19.2	5.5	19.2	0.0088	22.4
EWLM	0.9:0.75	3.3	4.2	2.4	0.0066	3.2
(3,3.22-6.22)	0.6:0.4	2.9	3.8	2.5	0.0063	2.9
θ = 0.20, σ_θ = 0.02	0.3:0.1	2.6	3.0	3.0	0.0055	4.1
Cliff-James-Strong	0.9:0.75	8.6	2.7	2.9	0.0033	4.3
(5,0-5,6-23,29-40)	0.6:0.4	6.2	2.6	3.6	0.0032	3.6
	0.3:0.1	4.1	2.6	7.8	0.0032	8.8
(10,0-10,11-27,36-50)	0.9:0.75	4.1	0.8	1.3	0.0010	1.9
	0.6:0.4	2.8	0.8	1.5	0.0010	1.5
	0.3:0.1	1.7	0.8	3.1	0.0009	3.4
(15,0-15,16-33,43-60)	0.9:0.75	3.1	0.4	0.8	0.0005	1.3
	0.6:0.4	2.1	0.4	1.0	0.0004	1.0
	0.3:0.1	1.2	0.4	2.0	0.0004	2.2
KRDM	0.9:0.75	1.7	1.6	1.0	0.0020	1.3
(5,6-15,24-40)	0.6:0.4	1.5	1.5	1.0	0.0019	1.2
θ = 0.05	0.3:0.1	1.4	1.3	1.5	0.0017	2.0
(10,11-20,31-50)	0.9:0.75	1.4	0.7	0.6	0.0007	0.8
θ = 0.05	0.6:0.4	1.2	0.7	0.7	0.0007	0.7
	0.3:0.1	1.0	0.6	1.0	0.0007	1.2
(15,16-26,38-60)	0.9:0.75	1.4	0.4	0.5	0.0004	0.7
θ = 0.05	0.6:0.4	1.2	0.4	0.5	0.0004	0.6
	0.3:0.1	1.0	0.4	0.9	0.0004	1.1

Note: The minimum measurable concentration (MMC) is defined as the concentration at which the relative standard deviation in the measurement is 20%, assuming the product of the detector efficiency and sampling flow rate is 1.0 (counts per disintegration-liters per minute).

Table 2. Values for RRDM data analysis for various optimized timing schemes.

$t_o, t_x - t_1, t_y - t_2$ (minutes)	k_{i1}	k_{i2}	k_{i3}	s
5,6-15,24-40				
i=1	0.04939	0.0	0.0	
i=2	-0.00600	-0.01500	0.01781	0.0187
i=3	0.00075	0.01742	-0.00502	
10,11-20,31-50				
i=1	0.03739	0.0	0.0	
i=2	-0.00464	-0.00681	0.00767	0.0120
i=3	0.00065	0.00970	-0.00284	
15,16-26,38-60				
i=1	0.03367	0.0	0.0	
i=2	-0.00423	-0.00390	0.00466	0.0075
i=3	0.00064	0.00660	-0.00220	